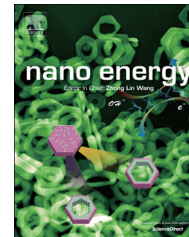




Available online at www.sciencedirect.com

ScienceDirect

journal homepage: www.elsevier.com/locate/nanoenergy



REVIEW

Heat flow at nanoparticle interfaces



Ronald J. Warzoha¹, Amy S. Fleischer*

Department of Mechanical Engineering, Villanova University, Villanova, PA 19010, USA

Received 28 December 2013; received in revised form 20 March 2014; accepted 22 March 2014
Available online 29 March 2014

KEYWORDS

Interfaces;
Nanoparticles;
Thermal boundary
resistance;
Substrate;
Matrix;
Phonon

Abstract

Nanoparticles are expected to significantly enhance future thermal energy generation systems, thermal energy storage materials, thermal interface materials and electronic devices. However, very few of these technologies are able to take full advantage of the unique thermal properties of nanoparticles, primarily due to the unusual transport phenomena that occur at their interfaces. To this end, a wealth of recent research has focused on the characterization and control of heat flow at different types of nanoparticle interfaces. The goal of this review is to provide critical insight into the mechanisms that govern thermal transport at three different types of nanoparticle interfaces, including: nanoparticle-substrate, nanoparticle-matrix and nanoparticle-nanoparticle interfaces. As part of this effort, we quantify the magnitude of heat flow at each type of interface using a collection of data that is available in the literature. This data is used to determine which physical mechanisms govern thermal transport at each different type of interface. Recent progress in the development of state-of-the-art thermal characterization techniques is also examined within the context of each type of nanoparticle interface. Finally, methods to control heat flow at different nanoparticle interfaces are discussed and future research needs are projected.

© 2014 Elsevier Ltd. All rights reserved.

Contents

Introduction	138
Fundamental heat flow physics at interfaces	138
Heat flow at nanoparticle-substrate interfaces	140
Heat flow physics at nanoparticle-substrate interfaces	140
Thermal metrology and interfacial thermal resistance at nanoparticle-substrate interfaces	142
Augmenting thermal transport at nanoparticle-substrate interfaces	144
Heat flow at nanoparticle-matrix interfaces	145

*Correspondence to: Villanova University, 800 Lancaster Ave., Villanova, PA 19085, USA. Tel.: +1 610 519 4996.

E-mail addresses: ronald.warzoha@villanova.edu (R.J. Warzoha), amy.fleischer@villanova.edu (A.S. Fleischer).

¹Villanova University, 800 Lancaster Ave., Villanova, PA 19085, USA.

Heat flow physics at nanoparticle-matrix interfaces	145
Thermal metrology and interfacial thermal resistance at nanoparticle-matrix interfaces	147
Augmenting thermal transport at nanoparticle-matrix interfaces	149
Heat flow at nanoparticle-nanoparticle interfaces	151
Heat flow physics at nanoparticle-nanoparticle interfaces.	151
Thermal metrology and interfacial thermal resistance at nanoparticle-nanoparticle interfaces.	152
Augmenting thermal transport at nanoparticle-nanoparticle interfaces.	154
Concluding remarks and perspectives for the future	155
Acknowledgment.	156
References	156

Introduction

The physics that occur at sub-micron length scales can be manipulated in order to produce remarkable improvements in the thermal, electrical, optical and mechanical properties of materials, allowing for the development of state-of-the-art thermoelectric devices, solar cells, battery electrodes, capacitors, advanced coatings and composite structures [1-6]. The extraordinarily wide range of thermal properties that have been achieved by nanostructuring materials is primarily due to the reduction in their characteristic dimensions to the point where quantum size effects and energy carrier scattering can be precisely controlled [7-9]. As a result, nanoparticles are beginning to transform future energy technologies [10].

The intrinsic thermal properties of individual nanoparticles have been manipulated and tuned to magnitudes that diverge significantly from the thermal properties of bulk materials [11,12]. For instance, carbon allotropes are typically found to exhibit high thermal conductivities in bulk due to the strong covalent bonds that exist between individual carbon atoms, which allow phonons to traverse through them at very high frequencies. The usual example of a bulk carbon allotrope with a very high thermal conductivity is diamond, whose tetrahedral lattice structure and sp^3 atomic bonds allow for high rates of phonon transport, even in the presence of internal phonon-phonon, phonon-electron and/or phonon-defect scattering. At the nanoscale, the chemical and physical mechanisms that govern heat flow in carbon allotropes are further enhanced. In these structures, sp^2 atomic bonds are formed between neighboring carbon atoms, which allow for even higher rates of phonon transport when compared to their bulk counterparts. Further, when the characteristic dimension of the nanoparticle is less than the mean free path of an energy carrier, its transport is considered to be ballistic (i.e. no internal energy carrier scattering exists). This phenomenon has led to the development of carbon-based nanoparticles having thermal conductivities that are measured to be higher than monocrystalline synthetic diamond [13]. Excellent reviews of the physical mechanisms that control heat flow within carbon nanoparticles are given in Refs. [14 and 15].

Alternatively, some nanoparticles are designed to possess extremely low thermal properties. These are exceptionally promising for use in thermoelectric devices and highly insulating composite materials. Researchers have computationally manipulated the grain boundaries and atomic defects within nanoparticles in order to increase internal boundary and Umklapp phonon scattering, thereby reducing heat flow rates

within the nanoparticle itself [16]. Nanoparticles have also been impregnated within bulk materials in order to disrupt harmonic phonon frequencies, which are shown to decrease thermal transport significantly [17]. An excellent review of heat transfer physics in low-dimensional systems with reduced thermal transport properties can be found in ref. [18].

While nanoparticles offer remarkably high or low intrinsic thermal properties, their integration into devices remains challenging from a thermal perspective. In typical devices, nanoparticles are often placed into contact with a substrate, another nanoparticle or are embedded within a host material (matrix). In this review, the mechanisms that govern heat flow at these junctions are discussed, and state-of-the-art methods to measure and control the phonon and/or electron scattering at nanoparticle interfaces are presented.

Fundamental heat flow physics at interfaces

Heat flow at interfaces remains an important topic in a wide variety of engineering disciplines, despite the abundance of research that has been conducted in this field to date. A thermal resistance (or the degree to which the flow of heat is impeded) is generally used to characterize heat flow at an interface (i.e. interfacial thermal resistance). The interfacial thermal resistance can be classified in two ways: (1) by thermal contact resistance and (2) by thermal boundary resistance (otherwise known as Kapitza resistance). Thermal contact resistance originates from mismatches in the surface conditions of two solid bodies and is an important parameter to quantify in electronics packaging, nuclear reactors, internal combustion engines and hypersonic flight vehicles [19,20]. An excellent review of thermal contact resistance at the nano scale can be found in Ref. [21]. In this review, we replace the term 'contact resistance' with 'constriction resistance' in order to better elucidate the role of the nano-sized length scales that are associated with nanoparticles.

Thermal boundary resistance is distinctly different from thermal contact resistance in that it still occurs over atomically 'smooth' interfaces. This form of interface resistance is dependent on the types of materials that are in contact with one another; here, one material's pertinent energy carriers (phonons/electrons) are 'deflected' at its geometric boundaries due to the differences in the electronic and acoustic properties of the contacting material, much the same way that rock formations 'scatter' (or break up)

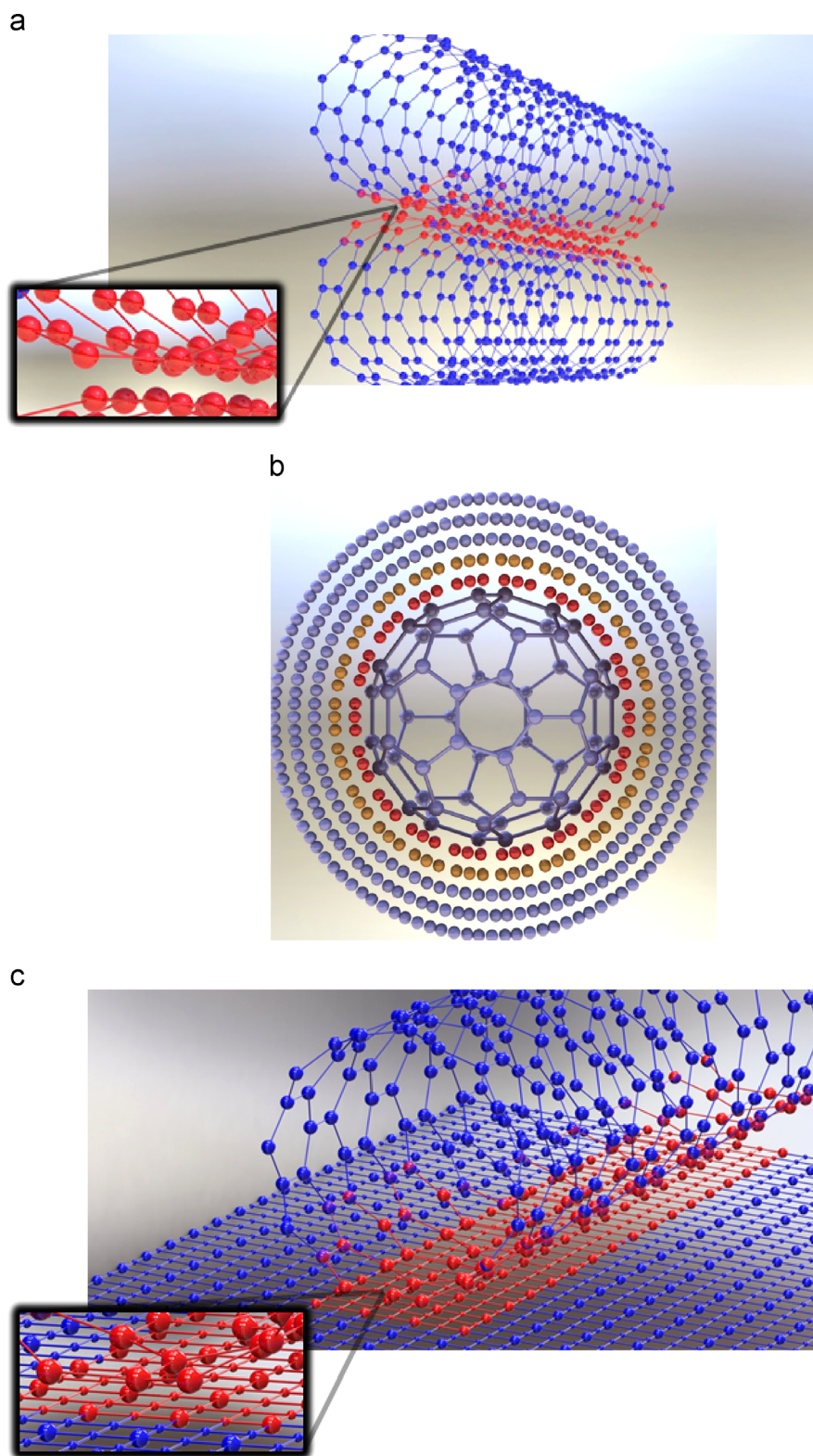


Figure 1 Contact morphology and heat flow between different nanoparticle interfaces: (a) nanoparticle-nanoparticle, (b) nanoparticle-matrix material and (c) a nanoparticle in contact with a substrate. Red coloring indicates an increased, non-dimensional temperature gradient at the interface. Figures are for illustration of the heat flow at nanoparticle interfaces only and are not to scale. (a) Contacting nanoparticles (two SWCNTs). (b) Nanoparticle embedded in a surrounding material (C60 fullerene surrounded by a highly ordered solid). (c) Nanoparticle in contact with a substrate (SWCNT on semi-infinite substrate of arbitrary material).

In Eq. (2), $U_{nanopatom\ substrateatom}$ is the van der Waals potential between a nanoparticle atom and a substrate atom, β represents the Lifshitz van der Waals constant and s is the distance between the nanoparticle and substrate atoms. The total van der Waals interaction force of all atoms acting upon one another in this arrangement is then computed according to Eq. (3).

$$F_{vdw} = -\frac{A}{\pi} \int_0^D \frac{\sqrt{(D-y)y}}{(y+l)^4} dy \quad (3)$$

In Eq. (3), A is the Hamaker constant ($N_s N_{np} \beta \pi^2$, where N_s and N_{np} are the number of substrate atoms and nanoparticle atoms, respectively, that interact with one another according to the geometry of Figure 2), D is the diameter of the nanoparticle (nm) and l is the characteristic dimension of the nanoparticle (nm). The line contact width (denoted by '2b' in Figure 2) can then be calculated by evaluating the elastic strain of the nanoparticle, which is based on the van der Waals contact force (Eq. (3)) [27]. The thermal constriction resistance at the interface is calculated based on a simple resistance analysis; that is, the individual nanoparticle thermal resistance, substrate thermal resistance and gap thermal resistance are calculated and summed in series. The gap thermal resistance is defined as the thermal resistance from the substrate through the surrounding medium (i.e. air, water, etc.) and subsequently into the nanoparticle. Each thermal resistance is defined in Eqs. (4)-(7).

$$R_{np} = \frac{1}{l_b \pi k_{np}} \ln\left(\frac{2D}{b}\right) - \frac{1}{2l_b k_{np}} \quad (4)$$

$$R_s = \frac{1}{l_b \pi k_s} \ln\left(\frac{D}{\pi b}\right) \quad (5)$$

$$R_{gap} = 2l_b k_f \left[\cot\left(\sin^{-1} \frac{2b}{D}\right) - \left(\frac{\pi}{2} + 1\right) \right]^{-1} \quad (6)$$

$$R_{constriction} = \frac{(R_{np} + R_s)R_{gap}}{(R_{np} + R_s) + R_{gap}} \quad (7)$$

In Eqs. (4)-(7), l_b is the length of the nanoparticle that is in contact with the substrate, k_{np} is the nanoparticle thermal conductivity, k_s is the substrate thermal conductivity and k_f is the thermal conductivity of the material in the gap between the nanoparticle and the substrate. It is clear that the model's accuracy relies heavily on determining the precise thermal conductivity of each relevant material. Additionally, while the development of this model accounts for both the adhesion energy and the size of the constriction that is formed between a nanoparticle and a semi-infinite substrate, it does not take into account any additional microscale physics that may affect thermal transport at the interface.

Prasher [28] reexamined the nature of this problem and modified the work of Bahadur et al. [27] to include the effects of additional microscale thermophysics at the interface between a non-metallic nanoparticle that is in contact with a non-metallic substrate. The author apportioned this work into three distinct physical models that are based on additional microscale thermophysics: (1) the diffusive limit when the phonon spectra between the nanoparticle and the substrate are equivalent (i.e. the characteristic dimension of the constriction is much larger than the phonon mean free path *and* the nanoparticle and substrate are composed

of the same material), (2) the ballistic limit when the phonon spectra between the nanoparticle and the substrate are equivalent (i.e. the characteristic dimension of the constriction is smaller than the phonon mean free path *and* the nanoparticle and substrate are composed of the same material) and (3) the ballistic limit when phonon spectra between the nanoparticle and the substrate are not equivalent (i.e. the characteristic dimension of the constriction is smaller than the phonon mean free path *and* the nanoparticle and substrate are composed of different materials). Eq. (8) defines the thermal constriction resistance between a non-metallic nanoparticle and a non-metallic substrate made of the same material when phonon transport occurs in the diffusive regime.

$$R_{constriction\ diffusive} = \frac{1}{4kb} \quad (8)$$

Eq. (8) is known as the Maxwell constriction resistance and is only dependent on the contact geometry between the nanoparticle and the substrate. Compared to the work done by Bahadur et al. [27], this represents an even simpler physical model and is accurate only for a handful of configurations due a lack of sufficient physics (such as the bonding energy between the substrate and the nanoparticle).

On the other hand, ballistic transport through the constriction allows for the unimpeded passage of phonons within or through a structure. For this case, Prasher [28] considers the flow of phonons through a constriction to be analogous to the flow of gas molecules through an orifice; in both circumstances, the mean free path of the pertinent energy carrier is significantly larger than the interface geometry. This simplified model reduces the complexity of phonon transport in that only acoustic phonons need to be considered, as the group velocity of optical phonons is very small relative to that of acoustic phonons. Considering transverse conduction only through the constriction ('2b' in Figure 2), the authors construct an energy balance that describes the heat flux at the nanoparticle-substrate interface in Eq. (9).

$$q = \frac{v_g}{4\pi} \sum_3 \int_0^{\omega_m} \int_0^{\pi/2} \int_0^{2\pi} \frac{\hbar\omega}{\exp(\hbar\omega/k_b T)} D(\omega) d\omega d\theta d\varphi \quad (9)$$

The heat flux shown in Eq. (9) (q) is based on the group velocity of the acoustic phonons, v_g (m/s), the phonon frequency, ω , the phonon density of states, $D(\omega)$, the polar angle θ and the azimuthal angle φ of the atomic arrangement of molecules within the material. Upon applying a temperature gradient across the junction along with using the traditional definition of contact resistance at an interface ($R_{contact} = (\Delta T)/qA$), Eq. (9) can be solved to produce a thermal constriction resistance at the nanoparticle-substrate interface when heat flow is considered to be in the ballistic regime. The result of this derivation is given in Eq. (10).

$$R_{constriction\ ballistic} = \frac{4l}{3k_e A} \quad (10)$$

As is shown in Eq. (10), heat flow in the ballistic regime is a direct function of the phonon mean free path, l (nm), the harmonic mean thermal conductivity at the constriction ($k_e = 2k_1 k_2 / (k_1 + k_2)$, W/mK) and the area of the constriction, A (nm²) when the nanoparticle and substrate are of the same material. In a comparison to the model developed by Bahadur et al. [27], Prasher [28] evaluates the same 1 μ m long Si

nanowire on a Si substrate and finds that the model developed by Bahadur et al. [27] significantly underestimates the contact resistance at the interface. This is because the constriction size formed by the Si nanowire and Si substrate is ~ 2 nm, whereas the mean free path of phonons in crystalline Si is ~ 250 nm. Thus, most of the thermal constriction resistance occurs in the ballistic regime rather than the diffusive regime.

A more accurate determination of the thermal constriction resistance can be obtained by summing the thermal resistances in both the diffusive and ballistic regimes. For a nanoparticle resting on a substrate of the same material, the thermal constriction resistance at the junction can be reduced to a form that is a function of the Knudsen number (l/a) such that when $Kn \rightarrow 0$, the thermal constriction resistance is dependent only on the diffusive phonon physics, whereas when $Kn \rightarrow \infty$, the thermal constriction resistance is only a function of ballistic phonon physics. This type of analysis helps to elucidate the pertinent physics associated with heat flow at the interface between a nanoparticle and substrate made of the same material. However, very rarely are these two materials the same when integrated into devices. Thus, it is imperative that additional physics be accounted for in an alternate model when dealing with dissimilar materials.

When the nanoparticle and substrate are composed of different materials, phonons will reflect at the boundary due to the differences in the vibrational harmonics between lattice structures. This reflection is expressed in terms of a transmission coefficient, α , and can be used to construct an energy balance in order to solve for heat flow across the interface. The heat flow can then be related to $R_{contact}$ (as was done for Eq. (10)) and the thermal boundary resistance can be extracted. Using these relations, the thermal boundary resistance (R_b) is calculated according to Eq. (11).

$$R_b = \frac{4}{\alpha_{1 \rightarrow 2} C_1 v_{g1}} \quad (11)$$

In Eq. (11), the thermal boundary resistance is a function of the transmission of phonons from material 1 to material 2 ($\alpha_{1 \rightarrow 2}$), the heat capacity of material 1 and the phonon group velocity of material 1. However, calculating R_b analytically is challenging due to the number of unknown parameters in Eq. (11), which often require experiment or great computational expense in order to determine their values where no analytical formulations are present. Thus, the development of a more accurate physical model describing the thermal boundary resistance at a nano-sized junction between two dissimilar materials will be critical for the successful integration of nanoparticles into future devices. Nevertheless, one can use an experimentally determined value of thermal boundary resistance in order to resolve the total thermal boundary resistance at a nano-sized interface between two dissimilar materials. As an example, the total interfacial thermal resistance across a circular constriction when phonon transfer occurs within the ballistic regime is given in Eq. (12).

$$R_{tot} = \frac{1}{2kA} \left[1 + \frac{2R_b k}{\pi 2b} \right] \quad (12)$$

In this section, heat flow through a nano-sized interface is shown to depend on three primary factors: (1) the area of the interface, (2) the strength of the bond between the nanoparticle and the substrate and (3) the phonon spectra

mismatch when two dissimilar materials come into contact with one another. It is also clear that the size of the interface dictates the phonon transport regime, which has a significant effect on heat flow across a nanoparticle-substrate junction. Additionally, when phonon transport is diffusive, the adhesion energy between the nanoparticle and the substrate is considered to be the dominant mechanism affecting heat flow at the interface. Finally, when the nanoparticle and substrate are not fabricated from the same material, the magnitude of phonon reflection at the junction is the most significant contributor to heat flow at the nanoparticle-substrate interface. These results suggest that the selection of materials and their geometries should have a significant impact on heat transfer in device architectures. However, while these analytical models (and other analytical/computational models [29]) describe the physics associated with semiconducting materials fairly well, there is still a need to develop more robust physical models that describe the interaction between phonons and electrons at metallic/metallic and metallic/semiconducting nanoparticle-substrate interfaces. Additionally, there have been relatively few theoretical studies that address modifications to the adhesion energy at nanoparticle-substrate interfaces. Until reliable methods for determining the interfacial thermal resistance across multiple, low-dimensional material combinations are developed, scientists will be forced to rely on either experiment or numerical simulation in order to extract the interfacial thermal resistance between a nanoparticle and a substrate.

Thermal metrology and interfacial thermal resistance at nanoparticle-substrate interfaces

The interfacial thermal resistance between a nanoparticle and a substrate has been measured in two ways: (1) using

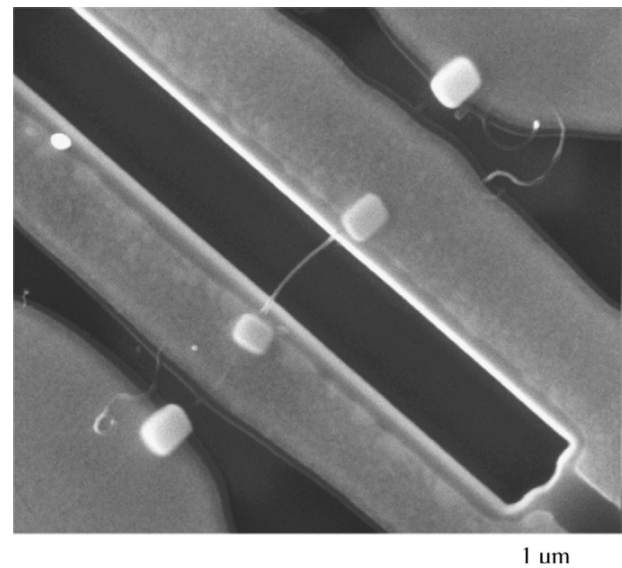


Figure 3 3- ω measurement apparatus for determining nanoparticle thermal conductivity and interfacial thermal resistance between a nanoparticle and a substrate. Figure adapted from ref. [30].

the 3- ω method and (2) using non-contact, optical methods.

The 3- ω method uses a set of microheaters/thermometers that act as both a heat source and heat sink in order to measure the thermal properties of a nanoparticle that is suspended across them. A current is applied to the circuit containing the metallic leads and the suspended material, and the voltage difference across the leads is measured using a Wheatstone bridge and lock-in amplifier. The nanoparticle's characteristic length, thermal conductivity and the nanoparticle-substrate contact area can then be used to calculate the thermal resistance at the nanoparticle-substrate junction. An example of a 3- ω device is shown in Figure 3 [30].

One disadvantage of this method is that it can only be used to measure the interfacial thermal resistance between a cylindrical nanoparticle and a substrate due to its geometrical constraints. Additionally, materials limitations restrict the use of this experiment to only a few nanoparticle-substrate combinations; in this case, the materials used to construct the leads must have well-defined temperature coefficients of resistance (such as platinum) in order to precisely measure the thermal transport rates across them. Despite its limitations, however, the 3- ω technique does allow for remarkable insight into the physics that control heat flow at different types of nanoparticle-substrate junctions.

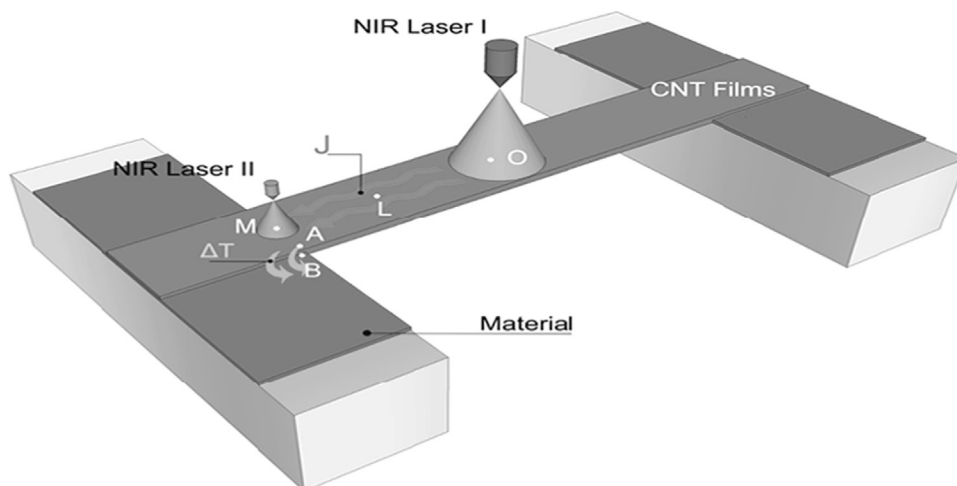


Figure 4 Non-contact technique for measuring interfacial thermal resistance between nanoparticles and a substrate. Figure adapted from ref. [31].

Table 1 Interfacial thermal contact resistance between different nanoparticle/substrate combinations.

No.	Nanoparticle type	Substrate material	T (K)	Contact width (2b) (nm)	Thermal boundary resistance (experiment) $m^2 K/W$	Reference
1	Carbon nanofiber ($d=125$ nm)	Pt	150	10.00 ^a	2.30×10^{-5}	[34]
2	Carbon nanofiber ($d=125$ nm)	Pt	300	10.00 ^a	1.21×10^{-5}	[34]
3	MWCNT ($d=25$ nm)	Cu	300	1.10	2.39×10^{-6}	[32]
4	MWCNT ($d=25$ nm)	Al	300	1.03	3.02×10^{-6}	[32]
5	MWCNT ($d=25$ nm)	Ni	300	1.08	2.28×10^{-6}	[32]
6	MWCNT ($d=25$ nm)	Au	300	1.31	3.95×10^{-6}	[32]
7	MWCNT ($d=25$ nm)	Ag	300	2.04	3.84×10^{-6}	[32]
8	MWCNT ($d=25$ nm)	Ti	300	0.96	2.76×10^{-6}	[32]
9	MWCNT ($d=25$ nm)	PMMA ^b	300	5.04	9.32×10^{-7}	[32]
10	MWCNT ($d=25$ nm)	EP ^b	300	- ^c	1.53×10^{-6}	[32]
11	MWCNT ($d=25$ nm)	S.E. ^b	300	- ^c	1.72×10^{-6}	[32]
12	MWCNT ($d=25$ nm)	PE ^b	300	5.09	1.79×10^{-6}	[32]
13	MWCNT ($d=25$ nm)	PET ^b	300	5.15	1.79×10^{-6}	[32]
14	MWCNT ($d=25$ nm)	PVC ^b	300	5.23	1.49×10^{-6}	[32]
15	InAs nanowire ($d=70$ nm)	Pt	350	1.70 ^a	3.51×10^{-7}	[35]
16	MWCNT ($d=14$ nm)	Pt	300	1.00 ^a	5.12×10^{-7}	[36]

^aExtracted directly from reference.

^bPMMA=Poly(methyl methacrylate), EP=Epoxy resin, S.E.=Silicone elastomer, PE=Polyethylene, PET=Poly(ethylene terephthalate), PVC=Poly(vinyl chloride).

^cInsufficient data available for analytical calculations.

An alternative way to measure the thermal resistance at nanoparticle-substrate junctions is to drive a heat flux through a series of aligned nanoparticles that are in contact with a substrate. To accomplish this, Li et al. [31,32] direct a laser at the midpoint of a nanoparticle array, the ends of which are in contact with different types of substrates. Once the system reaches a quasi-equilibrium state, a thermal resistance analogy is applied at the junction between MWCNTs and various substrates in order to extract a value for interfacial thermal resistance using Eqs. (13) and (14).

$$Q'_{nanoparticle} = \Delta T_{nanoparticle} / R_{nanoparticle} \quad (13)$$

$$R_{junction} = \frac{\Delta T_b}{\Delta T_{nanoparticle}} \left(\frac{A_{contact}}{A_{cross-section}} \right) \quad (14)$$

In Eqs. (13) and (14), $Q'_{nanoparticle}$ represents the steady-state heat flux across the nanoparticle array that is supplied by the laser, $\Delta T_{nanoparticle}$ is the temperature drop from point L to point M in Figure 4 (as measured by an infrared thermometer), $R_{nanoparticle}$ is the intrinsic thermal resistance along the length of the nanoparticles (L to M in Figure 4), ΔT_b is the temperature difference between points A and B in Figure 4, $A_{contact}$ is the real contact area between the nanoparticles and the substrate, $A_{cross-section}$ is the cross-sectional area of the nanoparticle sheet and $R_{junction}$ is the interfacial thermal resistance at the nanoparticle-substrate junction. Like the 3- ω technique, this technique is only suitable for relatively long, cylindrical nanoparticles. Additionally, the uncertainty of this method is substantially higher than the 3- ω technique due to the unknown number of nanoparticles that may come into contact with one another. However, it is significantly more economical to use than the 3- ω technique because it does not require any advanced nano scale manufacturing. Furthermore, when using this method to measure the interfacial thermal resistance between different substrates and the same type of nanoparticle, the results can reveal the significant physics at the nanoparticle-substrate interface.

In Table 1, experimentally obtained values of interfacial thermal resistance between different combinations of nanoparticles and substrates are given. In this table, the nanoparticles are held at the surface by van der Waals forces only. Thus, comparing these experimental values allows us to determine the effect of contact area and phonon spectra mismatch on thermal transport across a nanoparticle-substrate interface.

Tests 1 and 2 in Table 1 reveal the effect of temperature on the thermal boundary resistance between a carbon nanofiber and a platinum substrate. It is clear from this study that the thermal boundary resistance between a low-dimensional nanoparticle and a semi-infinite substrate is a strong function of temperature. This was confirmed by Zhang et al. [31], who found that both the trend describing thermal boundary resistance in this arrangement and the degree to which the thermal boundary resistance is a function of temperature vary greatly between different sets of nanoparticle/substrate combinations. A composite of this data is given in Figure 5, where the thermal boundary resistance is normalized against the intrinsic thermal resistance across the CNTs as well as the contact area between the CNT and the substrate. It is interesting to note that the carbon nanofiber-Pt substrate thermal boundary resistance is significantly higher than any

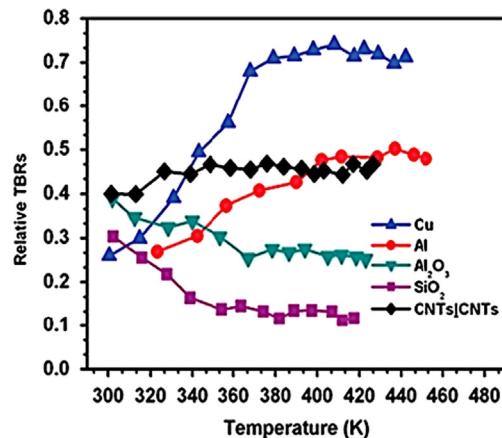


Figure 5 Temperature-dependent thermal boundary resistance at MWCNT-substrate junctions. Figure adapted from ref. [31].

of the other test samples in Table 1. This is potentially due to the higher dimensionality of the nanoparticle, which can lead to poor thermal transport at interfaces and, consequently, low rates of thermal enhancement within bulk materials and devices [33].

Tests 3-14 in Table 1 identify the effect of substrate material properties on the thermal boundary resistance at nanoparticle-substrate junctions. For the purely metallic substrates (tests 3-8), the contact geometry appears to have less to do with impeding heat flow than the substrate's thermophysical properties. According to Eq. (11), this effect is likely due to the discrepancy between the phonon group velocities of the MWCNT and each corresponding substrate material. For instance, the phonon group velocity in copper (4.6 km/s) is less than the phonon group velocity in aluminum (6.4 km/s), resulting in a higher interface resistance at the MWCNT-copper junction. When the Diffuse Mismatch Model is used to calculate $\alpha_{1 \rightarrow 2}$ with these group velocities, phonon transmission at the MWCNT-aluminum interface is nearly double that of the MWCNT-copper interface. Thus, the thermal boundary resistance at the MWCNT-aluminum interface is nearly half that of the MWCNT-copper interface according to Eq. (11). When one takes into account the discrepancy in the size of the constrictions between the two samples as well as the error associated with the Diffuse Mismatch Model, the results in Table 1 suggest that the greatest contributor to heat flow impedance at nanoparticle-metallic substrate interfaces is the mismatch in phonon spectra between the two materials. This is further elucidated when one examines the differences in the values of thermal interface resistance between metallic and polymer-based substrates, the conclusion of which is supported by studies that examine the nature of heat flow at polymer wrapped nanoparticle interfaces [37,38]. This remains true for the additional nanoparticle-substrate material combinations listed in Table 1.

Augmenting thermal transport at nanoparticle-substrate interfaces

The data in Table 1 suggest that thermal transport at nanoparticle-substrate junctions varies widely depending on both the nanoparticle and substrate materials that are in

contact with one another as well as the contact area at the interface. As a result, scientists are investigating ways to either mitigate or enhance the thermal impedance at this type of interface in order to increase the performance of different nanoparticle-substrate combinations for device applications. A survey of one interfacial heat flow enhancement technique is provided in Table 2.

Several groups have deposited an interstitial material (platinum) at the interface between a nanoparticle and a substrate in order to alter both the contact area and ‘phonon coherence’ at the junction. To date, this is the only technique whose heat flow performance enhancement has been measured at a nanoparticle-substrate interface. However, several other techniques are available for increasing the adhesion energy, contact area and phonon coherence at this particular interface, including: chemical functionalization [39], atomic layer deposition [40] and polymer wrapping [41,42]. Furthermore, the adhesion energy can be quantified using a nanoindenter with lateral force displacement, making it feasible to obtain accurate calculations of thermal boundary resistance as a function of the bonding strength between nanoparticle-substrate interfaces [43]. It is critical that these types of surface modifications be characterized and used for altering thermal transport at nanoparticle-substrate interfaces in the future.

Heat flow at nanoparticle-matrix interfaces

Nanoparticles are lightweight, have high surface area-to-volume ratios and exhibit a wide range of thermal properties, making them excellent candidates for use in next-generation composite materials [44], thermal interface materials [45] and thermal energy storage materials [46-50]. Several groups have found that the effective thermal conductivities of nanocomposites with very low volume fractions (up to 1 volume percent) are unusually high or low [51-53]. These results suggest that the physics that occur within these materials are much different at the nanoscale than the physics that occur in composite materials containing macro-sized

particles. In this section, we review the physics that control heat flow at the interface between a nanoparticle and a surrounding solid or fluid. Further, different thermal metrology techniques are reviewed; these techniques are allowing scientists to determine additional physics at nanoparticle-matrix interfaces and are critical for the development of next-generation nanocomposite materials and devices. Finally, the thermal boundary resistance between different types of nanoparticle-matrix interfaces, as well as techniques that are used to modify heat flow at this type of interface, are evaluated by using a selective collection of studies that are available in the literature.

Heat flow physics at nanoparticle-matrix interfaces

The interfacial thermal resistance between a nanoparticle and a surrounding matrix material is typically determined by finding a bulk nanocomposite’s effective thermal conductivity at different nanoparticle volume concentrations and subsequently applying a physical model to this data set. The physical models that relate the effective thermal conductivity to the nanoscale physics that control heat flow in nanocomposites typically include: (1) the intrinsic thermal properties of each material, (2) the geometry of the nanoparticle(s) and (3) the interfacial thermal resistance at the nanoparticle-matrix junction. Of course, the analytical models detailed in the section describing the thermal resistance between a nanoparticle and a substrate could be extracted to fit this condition; however, there is ambiguity in defining thermal transport within fluids at this length scale without resorting to the use of complex statistical thermodynamics. Instead, more general models are used to describe the physics at nanoparticle-matrix interfaces when the matrix is composed of a solid or a fluid [54-56]. Each of these models is detailed in Table 3 and many more have been reviewed extensively in the literature [57,58]. One additional model, developed by Nan et al. [59], has become the leading analytical tool used by scientists and engineers to date for extracting the nanoparticle-matrix thermal boundary

Table 2 Interfacial thermal contact resistance between different nanoparticle/substrate combinations and associated enhancement techniques.

No.	Nanoparticle type	Substrate material	T (K)	Contact width (2b) (nm)	Thermal augmentation technique	Thermal resistance (experiment) $m^2 K/W$	Relative enhancement ^a	Reference
1	Carbon nanofiber ($d=125$ nm)	Pt	150	50.00 ^b	Platinum deposition	1.90×10^{-5}	1.21	[34]
2	Carbon nanofiber ($d=125$ nm)	Pt	300	50.00 ^b	Platinum deposition	1.06×10^{-5}	1.14	[34]
15	InAs nanowire ($d=70$ nm)	Pt	350	8.78 ^b	Platinum deposition	1.81×10^{-7}	1.94	[35]
17	MWCNT ($d=14$ nm)	Pt	300	- ^c	Platinum deposition	3.07×10^{-7}	1.67	[36]

^aThermal resistance without enhancement-Thermal resistance with enhancement

^bExtracted directly from reference.

^cInsufficient information for calculation.

Table 3 Physical models used to determine nanoparticle-matrix interfacial thermal resistance. Rearranged from Refs. [54-56].

Model name	Model ^a	Nanoparticle type(s)	Reference
Hasselman-Johnson	$\frac{2K_m + K_p - 2\varphi(K_m - K_p) - K_e(2K_m + K_p + \varphi(K_m - K_p))/K_m}{K_e(2K_m K_p + K_m K_p \varphi/p)/K_m - 2K_m K_p/p + 2K_m K_p \varphi/p}$	Spherical	[54]
Prasher et al.	$\frac{2K_m + K_p - 2\varphi(K_m - K_p) - K_e(2K_m + K_p + \varphi(K_m - K_p))/K_m(1 + (PrRe/4))}{K_e(2K_m K_p + K_m K_p \varphi/p)/K_m(1 + (PrRe/4)) - 2K_m K_p/p + 2K_m K_p \varphi/p}$	Spherical	[55]
Nanda et al.	$\frac{d(K_p p \varphi / 3K_m((K_e/K_m) - 1) - p)}{2K_p}$	Cylindrical	[56]

^a K_m =matrix material thermal conductivity, K_p =nanoparticle thermal conductivity, φ =volume fraction of nanoparticles, p =nanoparticle aspect ratio, Pr =Prandtl number, Re =Reynolds number, d =nanoparticle diameter.

resistance due to its inclusion of many different factors, including complex geometries and nanoparticle orientation. As such, we briefly describe the significant physics associated with each of the models in Table 3 and provide an extended interpretation of the relevant physics included in the model developed by Nan et al. [59]. It should be noted that this discussion is different than that which describes the physics that dictate effective thermal conductivity of larger macro-scale nanocomposites; a discussion on the effective thermal conductivity of bulk nanocomposites necessitates the inclusion of several other types of physics, including Brownian motion [60], clustering [61,62], interparticle potential [63] and thermophoresis [64]. Instead, we focus on the interfacial physics associated with heat flow at nanoparticle-matrix junctions. As such, the Nan model will be used to extract the thermal boundary resistance between different nanoparticle-matrix combinations from the literature in the following sections.

Each of the equations in Table 3 can be used to compute the interfacial thermal resistance between an individual nanoparticle and a surrounding solid or fluid. In the first model, developed by Hasselman and Johnson, the thermal boundary resistance is primarily dependent on the aspect ratio of the nanoparticle, p , and the ratio of the intrinsic thermal conductivity between the nanoparticle and the surrounding fluid. In this equation (as well as with all others) the volume fraction (φ) can be used in order to extract R_b in tandem with simple experimentation. We describe this procedure in the next section. Conversely, the model developed by Prasher et al. [55] finds that the thermal boundary resistance between a nanoparticle and a surrounding matrix material is a function of Brownian fluid movement in close proximity to the nanoparticle, in addition to the physical mechanisms described by the Hasselman-Johnson model [54]. This model is only applicable for nanoparticle-fluid interfaces, while Brownian motion remains controversial in terms of its magnitude effect on thermal transport in bulk materials as well as at nano-sized interfaces. Finally, the model developed by Nanda et al. [56] reveals that the interfacial thermal resistance at a nanoparticle-matrix interface is primarily a function of the nanoparticle's geometry.

Recently, a benchmark study was conducted in order to assess the validity of different thermal characterization techniques and physical models for determining the effective thermal conductivity and nanoparticle-matrix thermal boundary resistance for different nanoparticle/matrix combinations [65].

The authors of this study found that the model developed by Nan et al. [59] most accurately captured the interfacial thermophysics between different nanoparticles and fluids. This model has also been used extensively in studies that examine the nature of heat flow between nanoparticles and solid matrix materials. As such, it is critical to include a detailed discussion of the pertinent physics that are described by this model.

The model developed by Nan et al. [59] is based on the assumption that an interstitial layer with thermal conductivity K_s , whose thickness is represented by δ , resides between a surrounding matrix material and the nanoparticle. This interstitial layer is realistically meant to represent different phenomena that impede heat flow between the matrix and the nanoparticle, including: (1) phonon spectra mismatch, (2) contact area, (3) adhesion at the interface and (4) the thickness and thermal transport of/through a disoriented layer of matrix material atoms that surround the nanoparticle. The authors begin their investigation of these physics by constructing a unit cell that contains a single nanoparticle, a surrounding matrix material and an interstitial layer. Given an elliptical nanoparticle of $i=n$ axes, Eq. (15) can be used to determine the axial equivalent thermal conductivity of the nanoparticle-interstitial layer-matrix composite.

$$k_{ii} = k_s \frac{k_s + L_{ii}(k_p - k_s)(1 - \nu) + \nu(k_p - k_s)}{k_s + L_{ii}(k_p - k_s)(1 - \nu)} \quad (15)$$

In Eq. (15), ν and L_{ii} are parameters that are a direct function of the nanoparticle's geometry [59]. Given that k_s and δ are not known *a priori*, Eq. (15) cannot be used to directly obtain the thermal boundary resistance between the nanoparticle and the matrix. However, by passing through the limit $\delta \rightarrow 0$ and $k_s \rightarrow 0$, Eq. (15) can be rewritten as Eq. (16).

$$k_{ii} = k_p / (1 + (\gamma L_{ii} k_p / k_m)) \quad (16)$$

In Eq. (16), γ is a function of interfacial thermal resistance, denoted by α_k , and the nanoparticle geometry [59]. The interfacial thermal resistance is defined in Eq. (17).

$$\alpha_k = R_{BD} k_m \quad (17)$$

In Eq. (17), R_{BD} is the thermal boundary resistance between the nanoparticle and the matrix and k_m is the thermal conductivity of the surrounding matrix material. Thus, one can extract the thermal boundary resistance based entirely on the thermal properties and geometry of the nanoparticle

and surrounding matrix material. Currently, this represents the most sophisticated model for describing the thermal boundary resistance between the nanoparticle and the surrounding matrix material. It is clear, though, that the phonon transport in the ballistic regime should be considered in order to further elucidate the role of nanoscale thermal transport at nanoparticle-matrix interfaces. Minnich and Chen [66] offer an initial formulation for the thermal boundary resistance at a nanoparticle-matrix interface in the ballistic regime; however, a comparison to experimental data is still needed for verification of the model, while additional insight into electron-phonon coupling at metallic interfaces should also be investigated. Nevertheless, we use the model developed by Nan et al. [59] in order to extract the thermal boundary resistance at nanoparticle-matrix interfaces in the studies that are used in the next section. We then compare this to state-of-the-art methods that are used to determine the interfacial thermal resistance at different types of nanoparticle-matrix interfaces.

Thermal metrology and interfacial thermal resistance at nanoparticle-matrix interfaces

The interfacial thermal resistance between an individual nanoparticle and a surrounding matrix material is conventionally determined by measuring the effective thermal conductivity of a dilute nanocomposite and applying the physical model developed by Nan et al. [59]. The effective thermal conductivity of different nanocomposite materials can be measured using a variety of different techniques, including: (1) the guarded hot-plate technique (for either solid or liquid nanocomposites) [67], (2) the transient hot-wire technique (for liquid nanocomposites, also known as nanofluids) [68], (3) the transient plane source technique (for either solid or liquid nanocomposites) [69,70], (4) the $3-\omega$ method (for liquid nanocomposites) [71], and (5) the laser flash thermal diffusivity technique (for either solid or liquid nanocomposites) [72]. These techniques vary in

accuracy and required measurement time, but all have been used extensively in the literature.

An illustration of the technique used to extract the thermal resistance at the nanoparticle-matrix interface with effective medium approximation is provided in Figure 6, which contains distributions of the effective thermal conductivity as a function of nanoparticle volume fraction and a corresponding linear curve fit that is used to extract the thermal boundary resistance. In this figure, ϕ_v represents the volume fraction of nanoparticles, ϕ_c is the critical volume fraction at which the nanoparticles begin to percolate, k_e is the effective thermal conductivity of the nanocomposite and k_m is the matrix material thermal conductivity. In a study conducted by Zhang et al. [73], SWCNTs were embedded within an epoxy in the dilute limit. If we apply a linear curve fit to the data, we can extract the thermal boundary resistance by comparing the equation obtained by the curve fit to the equation that models the thermal conductivity of randomly oriented cylindrical inclusions in ref. [66] and solve for R_b . A similar procedure was used to derive the thermal boundary resistance at the $\text{Al}_2\text{O}_3\text{-H}_2\text{O}$ interface in the work by Xie et al. [74]. At first glance, the data presented within this figure reveal that the thermal boundary resistance at a nanoparticle-matrix interface can vary substantially between different sets of nanoparticle-matrix combinations. To date, no single study has compared the results of multiple studies in order to observe the variances in thermal boundary resistance as a function of nanoparticle type, nanoparticle geometry and matrix material type. In this review, we provide a limited interpretation of some of the physical mechanisms that alter the thermal boundary resistance based on the aforementioned parameters. However, many additional studies are needed in order to quantitatively assess the influence of these parameters, and others, on interfacial heat flow at nanoparticle-matrix junctions with confidence.

An alternative method for determining the thermal boundary resistance at a nanoparticle-matrix interface is being used by a handful of research groups. This state-of-the-art technique uses transient absorption to measure the thermal boundary resistance at nanoparticle-matrix

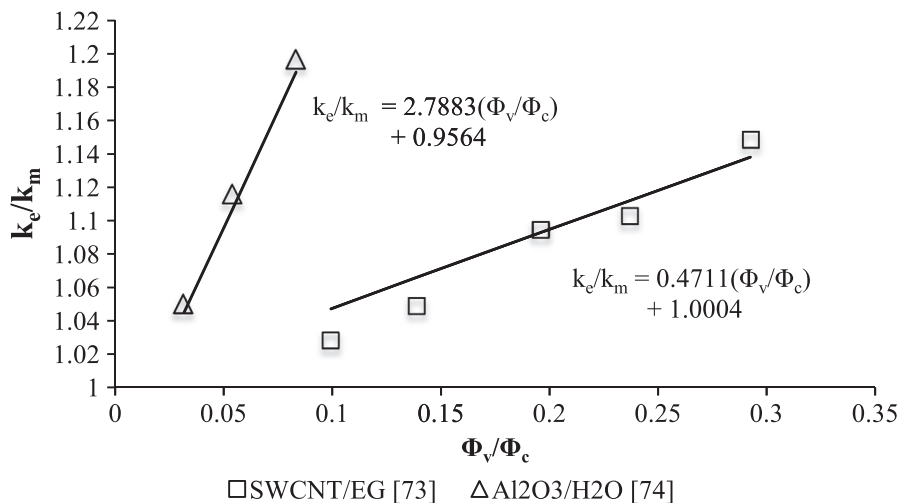


Figure 6 Technique for calculating thermal boundary resistance at nanoparticle-matrix interfaces using modified effective medium theory. Data extracted from refs. [73] and [74]. The transient hot-wire apparatus is used to measure the effective thermal conductivity of both types of nanoparticle suspensions in refs. [73] and [74].

interfaces. Transient absorption measurements are made using a modified modulated laser apparatus [75-77]. For this technique, the temperature decay of the nanoparticles after modulation is measured using a series of sub-picosecond pulses within relevant absorption spectra (graphene, for instance, exhibits absorption peaks within a wavelength range of $740 \text{ nm} > \lambda > 840 \text{ nm}$). The resulting temperature decay time can then be used to calculate the interface conductance (G) using Eq. (18):

$$\tau = C/AG \quad (18)$$

In Eq. (1), τ is the temperature decay time (ps), C is the heat capacity of the nanoparticle (J/K), A is the area of the nanoparticle (m^2) and G is the interface conductance ($\text{W}/\text{m}^2\text{K}$). Examples of the transient absorption distribution resulting from a single measurement are shown in Figures 7 and 8. Because the spatial resolution is on the order of nm, the interface conductance can be determined across different atomic layer configurations. For instance, if a surfactant is used to stabilize the nanoparticle so as to avoid nanoparticle settling, the interface conductance can be calculated for the nanoparticle-surfactant and surfactant-matrix interfaces by simply manipulating the absorption spectra. For example, this technique has been used to determine that the thermal contact conductance between a semiconducting CNT and a surfactant is significantly higher ($11.5 \text{ MW}/\text{m}^2\text{K}$) than between a metallic CNT and a surfactant ($9 \text{ MW}/\text{m}^2\text{K}$) [76]. In the future, this will also allow for further insight into the effect of heat flow across surface functional groups for tuning thermal transport at nanoparticle-matrix interfaces.

The interfacial thermal resistance at a sampling of seventeen total nanoparticle-matrix material junctions is shown in Table 4. The studies that were used to produce the

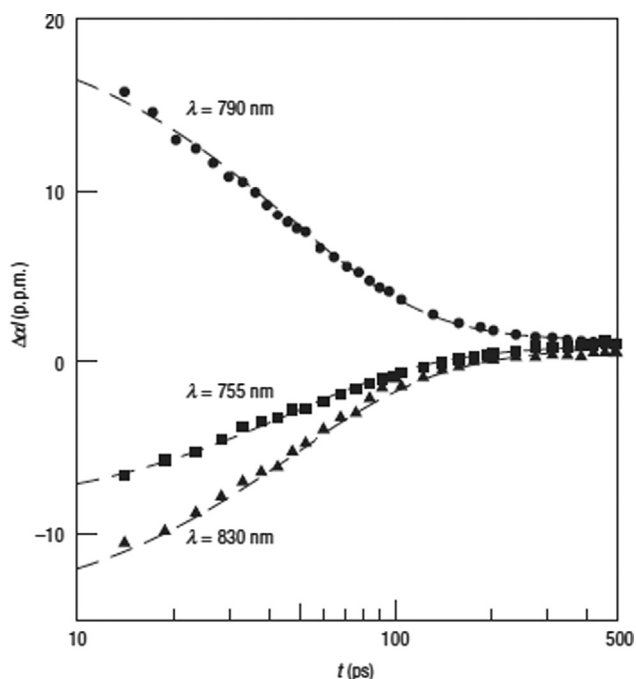


Figure 7 Example of absorption decay used to extract the thermal boundary resistance between a single nanoparticle and a surrounding matrix material using optical techniques. Extracted from Ref. [22].

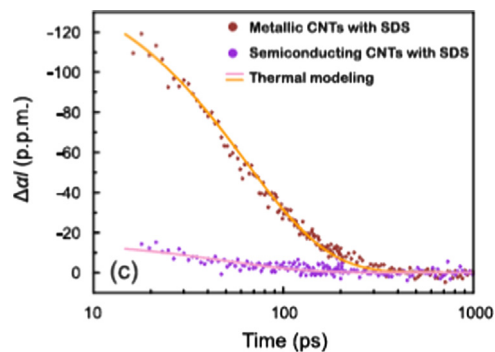


Figure 8 Example of absorption decay used to extract the thermal boundary resistance between a single nanoparticle and a surrounding matrix material using optical techniques. Extracted from Ref. [76].

data in Table 4 were chosen for this review based on two criteria: (1) the nanoparticles are within the dilute limit (i.e. they do not percolate) and (2) all dimensions and thermophysical properties of the nanostructures are supplied by the studies' authors. We could not find additional studies beyond those listed in Table 4 that met both of these criteria. In order to satisfy our first criterion, Eq. (19) was used to determine the volume fraction at which the nanoparticles begin to percolate (otherwise known as the critical volume fraction, ϕ_c) [78].

$$\phi_c = \frac{0.62}{p} \quad (19)$$

In Eq. (19), p represents the aspect ratio of the nanoparticle. For this work, only studies that include three or more data points at volume fractions below ϕ_c are used to extract the thermal boundary resistances in Table 4. The data in Table 4 appear to suggest that the thermal boundary resistance varies greatly as a function of nanoparticle geometry, type and materials combinations, which contradicts the results presented in a recent benchmark study that claimed the thermal boundary resistance at this interface is more or less independent of these parameters [65]. This discrepancy is potentially due to the wider range of sample types examined in this review. Additionally, significant error may result in [65] due an insufficient number of measurements for each type of nanoparticle (i.e. measurements must be taken for at least three volume loading levels in order to create a highly accurate linear best fit curve for the extraction of thermal boundary resistance; in many instances, measurements are reported at only two volume loading levels). Results for one of the most common nano-fluids ($\text{Al}_2\text{O}_3\text{-H}_2\text{O}$) suggest that the thermal boundary resistance at this type of interface can vary by over two orders of magnitude, which is well above the error associated with the individual measurement techniques and/or the curve fitting procedure used to solve for R_b . In this case, it is clear that the size of the nanoparticle has a marked effect on thermal boundary resistance, though it should be noted that none of these studies describe the surface conditions of the individual particles. It is therefore suggested that additional benchmarking studies be done in order to eliminate potential discrepancies in surface characteristics and to verify that the nanoparticle-matrix contact area can in fact have a

Table 4 Interfacial thermal resistance at different nanoparticle interfaces for selected nanoparticle composite materials.

Matrix material	Nanoparticle type	Nanoparticle shape	Nanoparticle diameter (nm)	Nanoparticle aspect ratio	Thermal boundary resistance ($\text{m}^2 \text{K/W}$)	Ref.
H ₂ O	Al ₂ O ₃	Spherical	36.0	1	1.8×10^{-8}	[79]
H ₂ O	Al ₂ O ₃	Spherical	20.0	1	1.0×10^{-8}	[73]
H ₂ O	Al ₂ O ₃	Spherical	47.0	1	1.9×10^{-9}	[80]
H ₂ O	Al ₂ O ₃	Spherical	45.0	1	1.3×10^{-8}	[81]
H ₂ O	Al ₂ O ₃	Spherical	60.4	1	2.0×10^{-10}	[74]
EG	SWCNT	Cylindrical	1.0	100	6.5×10^{-9}	[82]
EG	SWCNT	Cylindrical	1.2	300	2.4×10^{-9}	[83]
EG	Al ₂ O ₃	Spherical	50.0	1	3.0×10^{-9}	[84]
EG	Al ₂ O ₃	Spherical	45.0	1	3.2×10^{-8}	[81]
EG	Nanodiamond	Spherical	4.0	1	4.5×10^{-10}	[85]
Epoxy	SWCNT	Cylindrical	1.1	152	2.4×10^{-9}	[86]
Epoxy	Silica	Spherical	32.5	1	5.2×10^{-9}	[87]
Epoxy	FLG ^a	Plate	25.0 ^b	1200	6.8×10^{-7}	[88]
Paraffin	HGNF ^c	Cylindrical	100.0	1000	6.8×10^{-4}	[33]
Cu	MWCNT	Cylindrical	12.5	400	8.3×10^{-8}	[89]

^aFLG=Few Layer Graphene.

^bThickness.

^cHGNF=Herringbone Graphite Nanofiber.

two-order of magnitude effect on thermal transport at this type of interface.

A closer examination of Table 4 also reveals that the types of materials that are in contact with one another have a strong effect on the interfacial thermal resistance between them. For instance, when examining the SWCNT-matrix interfaces, one observes that the matrix material has a significant impact on thermal transport at the junction. Here, the SWCNT-H₂O thermal boundary resistance [22] is approximately $8.3 \times 10^{-8} \text{ m}^2 \text{K/W}$, whereas the thermal boundary resistance at both the SWCNT-ethylene glycol and SWCNT-epoxy interfaces is over an order of magnitude lower. These discrepancies highlight the strong effect of phonon spectra mismatch at the interface due to either a stronger molecular attachment between the matrix material atoms and the nanoparticle atoms, or a more ordered molecular arrangement at the nanoparticle-matrix boundary. Interestingly, the thermal boundary resistance is remarkably high for nanoparticles whose surfaces are not cylindrical or spherical. The thermal boundary resistance escalates considerably as the nanoparticle dimensionality increases based on the results for graphene nano platelets (2D) and graphite nanofibers (3D). Considering the relatively small sample size of the studies used to produce the data in Table 4, it is clear that additional experimental work is needed to reveal greater insight into the nature of heat flow across a nanoparticle-matrix material interface as a function of materials combinations, atomic arrangements and nanoparticle surface conditions.

Several studies have attempted to gain insight into these phenomena via atomistic simulations [90-96]. Xue et al. [95] used molecular dynamics simulations to determine the effect of liquid layering on thermal transport at a nanoparticle-liquid interface. The authors alter the strength of the bonding energy between liquid atoms in order to adjust the ordering

of the liquid at the interface. When a temperature gradient is imposed across the solid-liquid interface, the authors notice no difference in thermal transport as a function of the degree to which the liquid atoms are “ordered”, or arranged, at the interface. Thus, the authors theorize that the arrangement of atoms has little to do with thermal transport at the interface. In an additional study, the authors examine the role of intermolecular interactions between solid and liquid atoms on thermal transport at a nanoparticle-matrix interface [96]. Interestingly, the authors find that the bonding strength (or adhesion energy) between the solid and liquid atoms has a profound effect on thermal transport at the interface. Their results suggest that the thermal boundary resistance across the interface can be varied by nearly an order of magnitude over a relatively small range of adhesion energy between the solid and matrix-material atoms, which agrees relatively well with the analytical predictions made by Prasher [97]. While this result is promising, significantly more experimental measurements are required for its validation. It is suggested that future experimental studies examine the atomic arrangement and bonding strength at the interface using transmission electron microscopy (TEM) and micro-Raman/x-ray diffraction (XRD) studies, respectively, in tandem with state-of-the-art thermal characterization techniques (such as the optical absorption technique).

Augmenting thermal transport at nanoparticle-matrix interfaces

Recently, scientists have attempted to adjust interfacial heat flow by modifying the nanoparticles' surface conditions. A sampling of studies that have examined the role of nanoparticle surface characteristics on thermal transport at the nanoparticle-matrix interface is given in Table 5. Most

Table 5 Enhancement of thermal boundary resistance using surface modifications at different nanoparticle interfaces for selected nanoparticle composite materials.

No.	Matrix material	Nanoparticle type	Enhancement method	Nanoparticle diameter (nm)	Relative enhancement ^a	Ref.
1	Octane (polymeric)	SWCNT	Covalent attachment of octane molecules	0.7	3.40	[98]
2	Epoxy	FLG ^b	Nitric acid functionalization	25 ^c	1.25	[88]
3	H ₂ O	Silica	-OH functionalization ($n=8$) ^d	N/A ^e	0.92	[99]
4	H ₂ O	Silica	Self-assembled monolayers ($n=8$) ^d	N/A ^e	2.0	[99]
5	Silicone oil	MWCNT	HNO ₃ /NaOH and hexamethyldisiloxane	40	1.5	[100]
6	Mineral oil	Nanodiamond	Oleic acid (non-covalent)	11	50	[101]
7	H ₂ O	MWCNT	-COOH functionalization	100	40	[102]
8	Epoxy	MWCNT	-COOH functionalization	9.5	0.98-1.02 ^f	[103]
9	Epoxy	SWCNT	-COOH functionalization	2	0.014	[103]
10	Octane	FLG ^b	C ₈ -pyrene linker	N/A ^e	1.26	[104]
11	Poly(ethylene vinyl acetate)	SWCNT	Linear hydrocarbon chain attachments	N/A ^e	48	[105]
12	Epoxy	FLG ^b	Py-PGMA functionalization	2.3 ^c	200	[106]

^aThermal resistance without enhancement-Thermal resistance with enhancement.

^bFLG=Few-layer grapheme.

^cThickness.

^dMolecular chain length.

^eData extracted from molecular dynamics simulations without mention of diameter.

^fDifference in thermal resistance is within uncertainty of the measurement technique.

studies listed in Table 5 use functional groups that are attached covalently to a nanoparticle's surface in order to: (1) increase the surface area for heat transfer between the nanoparticle and the surrounding matrix material or (2) better match the vibrational spectra by linking molecular structures that are similar to the surrounding matrix material via covalent bond to the nanoparticle. The covalent bonds that are formed between the surface molecules and the nanoparticle are known to either form at defect sites or replace carbon atoms at the surface. The latter results in an sp³ bond at the interface where there was previously an sp² bond, which invariably decreases the intrinsic thermal conductivity of the nanoparticle [103]. However, it is possible that the reduction in thermal conductivity can be overcome by increasing the adhesion energy at the nanoparticle interface and/or by providing an interstitial material to bridge the different phonon spectra between the nanoparticle and the surrounding matrix material.

Studies 6 and 7 in Table 5 help to illuminate the difficulties in resolving the dominant physical mechanisms that control thermal transport at nanoparticle interfaces. In study 6, MWCNTs are functionalized with -COOH groups in order to better match the phonon spectra at the MWCNT-H₂O interface by providing a covalent bond between the MWCNT's carbon atoms and the hydrogen/oxygen atoms of the functional group, which closely match the phonon spectra of the surrounding matrix material. It is clear from this study that by matching the phonon spectra at the interface, a 40-fold reduction in thermal interface resistance is possible despite any reduction in the intrinsic thermal conductivity of the nanoparticle. This phenomenon is confirmed by the results

presented in studies 1-5. Study 7, however, contrasts these previous results; here, -COOH functional groups that are attached to the surface of different CNTs do not help to alleviate phonon spectra mismatch but instead increase it. This results in a significant reduction in thermal conductivity of the overall composite. When comparing studies 6 and 7, it is clear that the thermal transport at the interface (and thus the thermal transport within bulk nanoparticle-laden composites) can be tuned by controlling the interfacial surface conditions of the nanoparticle itself.

Non-covalent attachments also offer some control over thermal transport at nanoparticle-matrix material interfaces. In studies 8, 9 and 10, non-covalent linkers are attached to nanoparticle interfaces. Despite the weak adhesion energy at the interface, these studies suggest that the rate of thermal transport across the junction can be increased substantially by bridging the phonon spectra between the nanoparticle and surrounding matrix. Further, these studies show that it is possible to increase thermal transport across the interface by a large margin and within a wide range of values.

While it is undoubtedly possible to augment thermal transport at the nanoparticle-matrix material interface using surface functional groups, the thermal boundary resistance at the interface is predicted to span a range of over three orders of magnitude based on modifications to the adhesion energy at the interface alone. As a result, a great deal of additional work is needed to achieve precise tunability of thermal transport at both nano and macro-scale resolutions. Additionally, the magnitude effect of replacing sp² bonds with sp³ bonds on the intrinsic thermal conductivity of different types of nanoparticles must be studied in greater detail in order to

optimize the concentration of functional groups on nanoparticle surfaces in order to achieve high precision tunability of heat flow at the interface.

Heat flow at nanoparticle-nanoparticle interfaces

In next generation devices and materials, energy carriers are expected to traverse through contacting nanoparticles. The nanoparticles can be positioned such that the energy carriers are purposefully guided through pre-defined pathways, such as in integrated circuitry [107,108], and therefore constitute an integral part of next-generation technologies. There are some indications that the state-of-the-art materials necessary to implement these technologies are already available; however, it is critical that scientists understand how energy carriers traverse through different sets of nanoparticles in order for nanotechnologies to be included in future systems and devices. In this section, we review the pertinent physics associated with heat flow across the junction(s) of two or more contacting nanoparticles. We then review the state-of-the-art measurement techniques that are presently being used to determine the thermal boundary resistance at nanoparticle-nanoparticle interfaces and offer a summation of the experimental data that has been taken to date with respect to thermal boundary resistance. Finally, we examine several recent methods that have been developed in order to augment heat flow at this type of interface and project future needs in this area.

Heat flow physics at nanoparticle-nanoparticle interfaces

Here we present the physical models that are typically used to describe and calculate the thermal boundary resistance between two contacting nanoparticles. In the case of contacting nanoparticles, atomistic simulations are most often used to examine and extract the heat flow physics across interfacial regions [109-111]. Though atomistic simulations offer critical insight into the physics associated with heat flow at nanoparticle-nanoparticle interfaces, the pairwise potentials that are used to model the adhesion energy between the nanoparticles as well as the assumptions used for contact separation distance between the nanoparticles are difficult to validate with reasonable accuracy. This makes it difficult to resolve the dominant physical mechanisms that govern heat flow at this type of interface. Instead, we turn to analytical formulations that describe the physics associated with heat flow at nanoparticle-nanoparticle interfaces, which can easily be compared to experiment in order to determine the dominant physical mechanisms governing thermal transport across nanoparticle junctions.

Of course, the models developed by Bahadur et al. [27] and Prasher [28] can be used to analyze the nanoscale interfacial thermophysics across two individual, contacting nanoparticles. However, these models cannot be used to extract the thermal contact resistance/thermal boundary resistance at nanoparticle interfaces when using conventional experimentation. An alternative physical model that can be used to describe the interfacial heat flow at nanoparticle-nanoparticle interfaces is provided by Foygel et al. [112]. This model is typically used to

extract the interfacial thermal resistance in composites with randomly distributed, percolating networks of nanoparticles and therefore extends the range of experimental techniques that can be used to extract information about heat flow across a nanoparticle-nanoparticle junction.

The model developed by Foygel et al. [112] is primarily based on geometric relationships between the nanoparticle fillers, the morphology of the nanoparticle entanglement and the thermal conductance between nanoparticles. The authors first examine the macroscopic relationship between these parameters and the thermal conductivity of the bulk, percolating composite, which is represented by Eq. (20).

$$\sigma(\phi, a) = \sigma_0(\phi - \phi_c)^{t(a)} \quad (20)$$

In Eq. (20), σ thermal conductivity of the bulk nanocomposite, a is the aspect ratio of the nanoparticle(s), σ_0 is a preexponential factor that depends on the thermal conductivity and morphology of the contacting nanoparticles, ϕ_c is the critical volume fraction of nanoparticles and $t(a)$ is a conductivity exponent that is dependent on the aspect ratio of the nanoparticle. Eq. (20) can be iterated to find both σ_0 and $t(a)$ based on the application of a non-linear fit to the bulk thermal conductivity of the nanoscale composite as a function of volume fraction for a particular nanoparticle type. Using σ_0 and $t(a)$, the interfacial thermal resistance can be found according to Eq. (21).

$$R_0 = (\sigma_0 L \phi_c^{t(a)})^{-1} \quad (21)$$

Thus, according to Foygel et al. [112], the interfacial thermal resistance between contacting nanoparticles is wholly dependent on the cluster density (morphology) of the nanoparticle network (or the geometry of the junction that is formed between nanoparticles), the geometry of the individual nanoparticles and the thermal properties of the nanoparticles and the host material.

An alternative to the model developed by Foygel et al. [112] is the model developed by Wemhoff [78]. Despite its robustness and wide applicability, the model developed by Foygel et al. [112] does not allow for one to resolve the independent effects of nanoparticle-nanoparticle interfacial thermal resistance and nanoparticle-matrix interfacial thermal resistance. Further, the use of arbitrary coefficients and exponential factors to represent multiple parameters does not help to elucidate the effect of those parameters on thermal transport at the interface (i.e. the effects are confounding without appropriate physical models for σ_0). This makes it difficult to understand how further modifications to the interface, such as the adjustment of the adhesion energy between nanoparticles, affects heat flow across the nanoparticle-nanoparticle junction. Several others have used numerical and analytical approaches that make it similarly difficult to resolve the magnitude effect of additional parameters such as adhesion energy, but still give general insight into the physical mechanisms that govern heat flow across nanoparticle structures [113,114].

Instead, Wemhoff [78] has developed a physical model that is based on microscale physics associated with phonon transport within and across sets of randomly oriented, contacting, cylindrical nanoparticles. To begin, the author determines the average distance between intersecting nanoparticles based on the geometry of the inclusions and the phonon group

velocity attributed to the nanoparticle, as given in Eq. (22).

$$\lambda \approx \frac{v_g t}{\zeta \tau} = \frac{\pi}{4LDn} \quad (22)$$

In Eq. (22), v_g represents the phonon group velocity attributed to the nanoparticle, t is the total time a phonon exists in transit intrinsically within a nanoparticle, ζ is the nanoparticle-nanoparticle intersection frequency, λ is the average distance between intersecting nanoparticles, L is the length of the nanoparticle, D is the diameter of the nanoparticle and n is the number of nanoparticle inclusions present within the matrix. Using Eq. (22), the equivalent thermal resistance between inclusions is written in Eq. (23).

$$R_{np-np} = \overline{A_s} \left[\frac{k_{pe} A'_c}{\lambda} - \frac{k_p A'_c}{\lambda} \right] \quad (23)$$

In Eq. (23), R_{np-np} is the inter-nanoparticle thermal resistance, $\overline{A_s}$ is the average overlap area between contacting nanoparticles, k_{pe} is the bulk thermal conductivity of the nanoparticle set (or network), k_p is the intrinsic thermal conductivity of the nanoparticle and A'_c is the nanoparticle cross-sectional area. Thus, the interfacial thermal resistance is dependent on the geometry of the nanoparticle, the intrinsic thermal conductivity of the nanoparticle and the phonon-dominated scattering events within the nanoparticle network.

In the following section we detail the thermal metrology associated with resolving heat flow at nanoparticle interfaces experimentally. The different physical models described in this section will then be used to determine the interfacial resistance at different types of nanoparticle interfaces. Both models are used to determine the interfacial thermal resistance at nanoparticle-nanoparticle junctions for experiments that measure heat flow through composites with embedded, percolating nanoparticle structures, while new state-of-the-art methods utilize the physics associated with the models developed by Bahadur et al. [27] and Prasher [28] in order to resolve the magnitude of heat flow at the junction between nanoparticles. The data generated in the next section will be used to quantitatively assert the dominant mechanisms that are responsible for heat flow across individual nanoparticle junctions.

Thermal metrology and interfacial thermal resistance at nanoparticle-nanoparticle interfaces

For most of the work considered here, the methods used to extract the interfacial thermal resistance between contacting nanoparticles are the same that are used to determine the interfacial thermal resistance between a nanoparticle-matrix interface; that is, conventional techniques such as laser-flash, transient hot-wire and guarded hot plate are used to determine the thermal conductivity of composite materials with randomly oriented, contacting nanoparticles and physical models (like the Foygel et al. [112] and Wemhoff [78] models) are subsequently used to extract the interfacial thermal resistance at nanoparticle interfaces. Thus, in this section we review only the state-of-the-art methods that are used to quantify heat flow at the nanoparticle-nanoparticle interface.

Although significant insight into the heat flow physics at nanoparticle-nanoparticle interfaces can be gained by

utilizing the standard techniques described previously, there is some variability in nanoparticle size distribution, nanoparticle orientation, etc., that result in a reasonable degree of error in predicting the TBR at this type of junction. In order to minimize this error, researchers have turned to the 3- ω technique, which has traditionally been used to measure the thermal conductivity of individual nanoparticles. In a seminal study, Yang et al. [115] determine the thermal contact resistance between two individual multiwalled carbon nanotubes with the 3- ω technique. The authors utilize two SiN_x membranes with integrated platinum leads to serve as a heat source/sink network and subsequently suspend two individual MWCNTs across them. The MWCNTs are placed into contact with one another in two different orientations (in-plane, where the nanoparticles overlap one another along a line segment of atoms, and cross-plane, where the nanoparticle are oriented perpendicularly to one another and contact over a small, circular area) in order to determine the effect of contact orientation on heat flow between sets of nanoparticles. Scanning Electron Micrographs of the apparatus used for this test are shown in Figure 9. The goal of this study is to determine the optimal orientation for nanoparticles to contact one

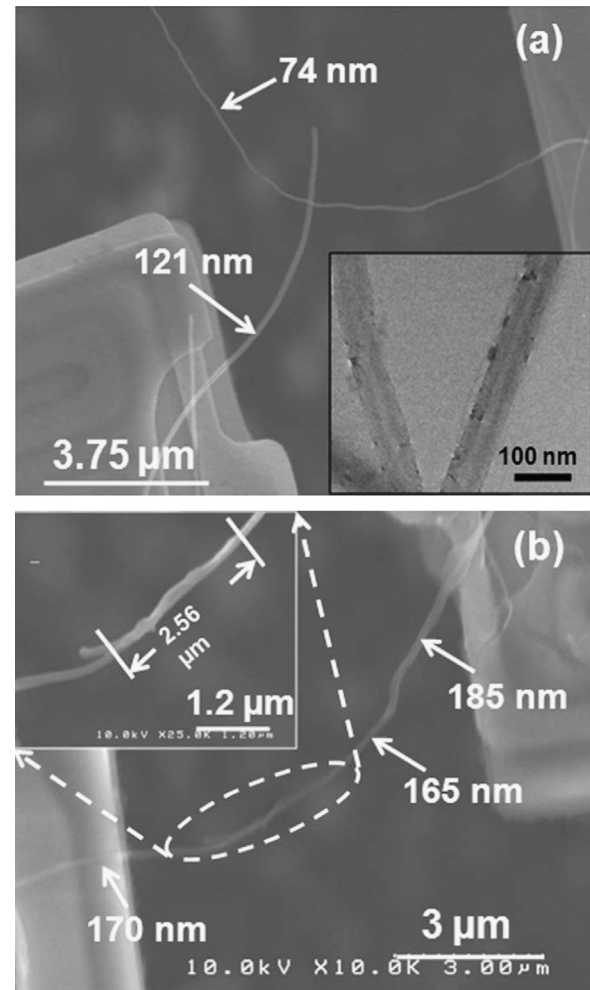


Figure 9 SEM micrographs of two CNTs in contact with each other in the following orientations: (a) cross-plane and (b) in-plane. Figure adapted from ref. [115].

Table 6 Interfacial thermal resistance at different nanoparticle-nanoparticle junctions.

Nanoparticle type	Matrix type	Nanoparticle shape	Nanoparticle average diameter (nm)	Nanoparticle aspect ratio	Thermal contact resistance ($\text{m}^2 \text{K/W}$) (Foygel)	Model fit parameters ($\sigma_0 t(a)/A_c$) ^a	Thermal contact resistance ($\text{m}^2 \text{K/W}$) (Wemhoff)	Model fit parameters (R_{np-m}/k_{np}) ^b	Ref.
Aligned MWCNTs (transverse direction)	Epoxy	Cylindrical	8	~125,000	N/A	N/A	1.02×10^{-8}	1.00×10^{-11} 5.42	[116]
Aligned MWCNTs (axial direction)	Epoxy	Cylindrical	8	~125,000	N/A	N/A	1.02×10^{-9}	1.00×10^{-11} 452	[116]
SWCNTs	PMMA	Cylindrical	1.5	666.77	1.41×10^{-8}	27 1.5 0.00001	N/A	N/A	[117]
SWCNTs	High density polyethylene	Cylindrical	3	148	1.37×10^{-8}	36 1.6 0.00003	N/A	N/A	[118]
MWCNTs	PDMS	Cylindrical	15	5000	2.54×10^{-9}	350 1.2 0.0013	2.24×10^{-9}	5×10^{-11} 538	[119]
HGNF ^c	Paraffin (Solid)	Cylindrical (3D)	100	1000	5.40×10^{-5}	20 1.4 0.04	N/A	N/A	[33]
Graphene	Hexadecane (Liquid)	Platelet (2D)	5	200	2.40×10^{-6}	4000 1.7 0.00009	N/A	N/A	[120]
Graphene	Hexadecane (Solid)	Platelet (2D)	5	200	2.20×10^{-6}	9000 1.8 0.00009	N/A	N/A	[120]
Few layer graphene	Nylon-6	Platelet	7.5	1500	1.33×10^{-7}	250 1.8 0.0003	N/A	N/A	[121]

^aUnits of σ_0 are W/m K , $t(a)$ is a fitting parameter depending on the morphology of nanoparticle clusters, A_c =avg. contact area (μm^2).

^b $R_{np-matrix}$ =Nanoparticle-matrix thermal boundary resistance, k_{np} =nanoparticle thermal conductivity.

^cHGNF=Herringbone Graphite Nanofiber.

another in percolating composites in order to achieve the highest bulk thermal conductivity of the composite. The authors find that the interfacial thermal resistance between individual MWCNTs is on the order of 10^{-9} m² K/W and that aligned contact offers a nearly two order of magnitude increase in the heat flow rate between nanoparticles than does cross-contact, likely due to the available area for heat transfer at the junction. However, while the results of this work offer a basis for designing composite materials for optimal thermal performance, the most important feature of this study is its novelty in experimentally determining the interfacial thermal resistance between individual, contacting nanoparticles. The significance of this work can not be understated and should lead to more accurate findings for interfacial thermal transport between nanoparticles, including greater insight into the physical mechanisms that control thermal transport at the nanoparticle-nanoparticle junction.

In order to understand the parameters that affect heat flow at the nanoparticle-nanoparticle interface, we apply the physical models detailed in the previous section to the data supplied in seven total data sets that we found in the literature [116-121]. The results are presented in Table 6. The criteria used for selecting the data are as follows: (1) if the standard technique is used to extract the interfacial thermal resistance, the data set must contain at least four data points that are beyond the percolation threshold, (2) if the standard technique is used to calculate the interfacial thermal resistance, all geometrical properties, including the nanoparticle diameter and length/thickness, must be provided by the author(s) and (3) if the $3-\omega$ technique is used, the authors must have accounted for the TBR at the nanoparticle-substrate interface. We also note that the data in Table 6 only represent a fraction of the data that is available in the literature; we choose to incorporate only enough data to illustrate the dominant physical mechanisms governing thermal transport at the nanoparticle-nanoparticle interface. Where possible, a secondary data set is used to confirm the phenomena revealed by the original data. Finally, both the Foygel et al. model [112] and the Wemhoff model [78] are used to extract the interfacial thermal resistance between nanoparticles where appropriate. We note that for the Foygel et al. model [112], it is necessary to multiply R_0 by the average contact area at the nanoparticle-nanoparticle junction in order to compare the interfacial thermal resistances between groups. To calculate the average contact area between nanoparticles, we use the methods developed by Wemhoff [78].

For the first two nanoparticle types listed in Table 6, we apply the Wemhoff model [78] to the data provided by Marconnet et al. [116] in order to extract the thermal contact resistance between aligned MWCNTs that randomly link together at sidewall locations. Although the Wemhoff model [78] was developed for randomly oriented cylindrical nanoparticles, the random linking of the vertically aligned nanoparticles (as is typically found in many common arrangements [122-124]) allows for the use of this model to determine the magnitude of heat flow at the interface. The data suggest that the thermal contact resistance between MWCNTs is on the order of $\sim 1 \times 10^{-8}$ m² K/W. The Wemhoff model [78] also predicts the thermal conductivity of the individual MWCNTs within the surrounding matrix material with remarkable accuracy. In this case, the model predicts an axial MWCNT thermal conductivity of 452 W/m K and a transverse MWCNT thermal conductivity of

5.42 W/m K, which are consistent with experimentally measured values that are presented in the literature [125]. Similar results are found for SWCNTs that are randomly dispersed within polymer matrices [117,118]. However, nearly an order of magnitude reduction in interfacial thermal resistance is found when much larger MWCNTs come into contact with one another [119]; in this case, the average contact area between the MWCNTs is significantly greater than in each of the previously mentioned studies. This supports the theory that the size of the constriction between contacting nanoparticles can have an enormous effect on the thermal transport between them. Finally, it seems that the dimensionality of the nanoparticle has an enormous effect on the interfacial thermal resistance across nanoparticle junctions. In one study (which was conducted by the authors of this paper), the thermal contact resistance between sets of three-dimensional nanoparticles (HGNF) is shown to be four to five orders of magnitude higher than between sets of SWCNTs and MWCNTs [33]. Considering that this analysis normalizes against the nanoparticles' intrinsic thermal conductivities ($k_{HGNF}=25$ W/m K [126], $k_{SWCNT}=3000$ W/m K [125]), this result is striking. Further proof of this phenomenon is found in the results presented by Zheng et al. [120], whose two-dimensional graphene nanoparticles exhibit a thermal contact resistance that is on the order of 10^{-6} m² K/W. This is two orders of magnitude higher than the one-dimensional SWCNTs in references 117 and 118, and two orders of magnitude lower than the three-dimensional HGNF used in ref. [33]. Although these data do provide some insight into the physical mechanisms that control heat flow between nanoparticles (i.e. size effects, nanoparticle dimensionality), a larger compilation of data is needed for both confirmation and further insight into the effects of contact area and phonon spectra matching at nanoparticle-nanoparticle junctions. We note here that in order to do this in the future, research groups must report all of the relevant geometries and thermophysical properties of the individual materials that are in contact with one another, as well as report on the effective thermal conductivity of 4 or more volume fractions of nanoparticles in percolating composite materials.

Augmenting thermal transport at nanoparticle-nanoparticle interfaces

Interfacial thermal transport between contacting nanoparticles has long been of interest to the scientific community. However, efforts to augment thermal transport between contacting nanoparticles is widely considered to be an emerging frontier in the fields of thermophysics and heat transfer. As a result, only a limited number of research publications exist in the literature that address heat flow augmentation at nanoparticle-nanoparticle interfaces. Further, we could find only one study that can be used to analyze the physics of heat flow across the junction between nanoparticles. We have compiled the data from this study into Table 7 in order to illustrate the effect of surface modifications to nanoparticles on the thermal transport between them. The interfacial thermal resistance between nanoparticles is quantified using both the Foygel et al. [112] and Wemhoff [78] models described in the previous section. The data in Table 7 offer promising results for future developments of nanoparticle-nanoparticle

Table 7 Augmentation of thermal transport at nanoparticle-nanoparticle interfaces using nanoparticle surface modifications.

Nanoparticle type	Matrix type	Surface modification	Nanoparticle shape	Nanoparticle average diameter (nm)	Nanoparticle aspect ratio	Thermal contact resistance (m ² K/W) (Foygel)	Thermal contact parameters (σ ₀ t(a) A _c) ^a	Thermal contact resistance (m ² K/W) (Wemhoff)	Model fit parameters (R _{np-m} k _{np}) ^b	η ^c	Ref.
Graphene	Epoxy	Amine functionalization	Platelet	50	68	1.18 × 10 ⁻⁷	250 2 0.008	N/A	N/A	1.6	[127]

^aUnits of σ₀ are W/m K, t(a) is a fitting parameter depending on the morphology of nanoparticle clusters, A_c=avg. contact area (μm²).

^bR_{np-matrix}=Nanoparticle-matrix thermal boundary resistance, k_{np}=nanoparticle thermal conductivity.

^cη= surface functionalization efficiency (TCR_{nanoparticles with surface enhancement in matrix}-TCR_{nanoparticles in matrix only}).

systems using surface modifications; in this case, the grafting of amine groups onto the outer layers of graphene allow for increased adhesion energy between the nanoparticles, which results in a 160% increase in thermal transport across them [127].

While there is insufficient data to determine the dominant physical mechanisms that control heat flow across nanoparticle-nanoparticle junctions when nanoparticle surfaces are modified, there are alternative studies that qualitatively suggest that the thermal transport between nanoparticles has been altered significantly. In one study conducted by Gulotty et al. [103], the thermal conductivity of an MWCNT/epoxy composite in the percolating regime was shown to decrease with increasing -COOH functional groups. Although these functional groups have been shown to increase the thermal conductivity of other carbon nanoparticle-based composites, this study suggests that an oversaturation of -COOH groups on the MWCNT surface may lead to too large a degradation in the intrinsic thermal conductivity of the MWCNT to overcome the benefits of increased adhesion energy and phonon spectra coherence at the MWCNT-MWCNT interface. This is because for each functional group attachment, one sp³ atomic bond is eliminated in favor of an sp² atomic bond, thereby reducing the high rate of heat transfer within the MWCNTs due to the original sp³ bonds. Other studies [128,129] involving boron nitride nanoparticles offer varying perspectives on the ability to augment thermal transport at nanoparticle-nanoparticle interfaces by modifying the adhesion energy, contact area and/or phonon spectra at the surface. Thus, due to the limited number of results that are used to analyze interfacial thermal transport between nanoparticles, additional benchmark studies and research are needed before making definitive conclusions about the effect of these parameters on thermal transport across nanoparticle-nanoparticle interfaces.

Concluding remarks and perspectives for the future

In this review, the heat flow physics, thermal metrology and interfacial thermal resistance are examined for three different types of nanoparticle interfaces: (1) nanoparticle-substrate interfaces, (2) nanoparticle-matrix interfaces and (3) nanoparticle-nanoparticle interfaces. These interfaces are particularly important for the development of next-generation electronic devices, renewable energy systems and materials.

In the first part of this review, the heat flow physics at nanoparticle-substrate interfaces are presented and analyzed. In early studies, the geometry of the constriction formed between the substrate and the contacting nanoparticle (i.e. the contact area) is used as the foundation for analyzing heat flow across nanoparticle-substrate junctions. However, because the characteristic dimension of the constriction is on the order of the mean free path of phonons for most materials, this type of diffusive analysis is found to be insufficient for the accurate prediction of heat flow between a nanoparticle and a substrate. Instead, both ballistic and diffusive heat flow are considered in tandem with the geometry at the interface, which is found to model heat flow across the nanoparticle-substrate junction with a high degree of accuracy when both the substrate and the nanoparticle are made of the same type of material.

When the two materials are different, however, it is necessary to account for phonon reflection at the interface in order to accurately capture the heat flow physics between them. When using these models to analyze the data that are available in the literature, thermal transport is heavily affected by the vibrational mismatch between the nanoparticle and substrate materials (more so than the contact area between the materials). Attempts to modify nanoparticle-substrate interfaces using platinum deposition have been made in order to mitigate phonon scattering between the materials due to this vibrational mismatch; however, the degree to which increasing the adhesion energy at the junction affects thermal transport varies between studies by as much as two orders of magnitude. Thus, there is a significant need for additional work to be done in this area in order to determine the relevant phonon physics that can be manipulated in order to tailor heat flow across different types of nanoparticle-substrate junctions.

Nanoparticle-matrix interfaces are expected to exist in a remarkably large number of materials and devices in the near future. In this review, we examine the nature of heat flow at these interfaces and subsequently analyze the data that are available in the literature in order to determine the dominant transport mechanisms that affect thermal transport at this type of junction. Typically, the interfacial thermal resistance at the nanoparticle-matrix interface is obtained by saturating a matrix with nanoparticles at a volume loading level that is below the percolation threshold (i.e. the nanoparticles are evenly dispersed and not in contact with one another). By evaluating the effective thermal conductivity of the nanoparticle-matrix bulk composite material for at least three distinct volume fractions below the percolation threshold, the data can be compared to any number of existing effective medium formulations and an interfacial thermal resistance can be extracted. While this technique is often associated with significant error, it has allowed scientists to gain significant insight into the mechanisms that govern heat flow between a nanoparticle and a surrounding matrix. Scientists have also developed an alternative, optical pump-probe technique that can determine the interfacial thermal resistance across a single nanoparticle. Although only a handful of studies have effectively utilized this technique to date, it does offer the promise of greater insight into the governing physics across a nanoparticle-matrix interface. When analyzing the data available in the literature, we find that the contact area between a nanoparticle and a matrix material can have up to a two-order of magnitude effect on interfacial heat flow. Additionally, both the types of materials that are in contact with one another and the dimensionality of the nanoparticle itself can have an enormous effect on thermal transport across the nanoparticle-matrix junction. Attempts to control the surface conditions of the nanoparticles in order to increase both the adhesion energy between the nanoparticles and the surrounding matrix material as well as the vibrational harmonics between the materials can lead to as much as a 200-fold increase in the thermal transmission at this interface as well. It is expected that these surface modifications will open a diverse area of research in the future and could potentially help to realize the full benefits of incorporating nanoparticles with high or low thermal conductivities into bulk materials.

Finally, in this review we analyze the flow of heat between two contacting nanoparticles. Similar to the way that we obtain

heat flow at the nanoparticle-matrix interface, physical models are often applied to data sets (having four or more data points) that evaluate the effective thermal conductivity of nanoparticle composites having randomly oriented nanoparticles at volume fractions that are above the percolation threshold. However, the $3-\omega$ technique has recently been used to evaluate the thermal contact resistance between two individual nanoparticles with great accuracy, which should offer improved insight into the heat flow physics at nanoparticle-nanoparticle interfaces in the future. For this review, we apply the physical models that describe the heat flow physics at nanoparticle-nanoparticle interfaces in order to determine the thermal contact resistance between the same types of nanoparticles. We find that both the contact area and the dimensionality of the individual nanoparticle can have up to a four order of magnitude effect on thermal transport at the nanoparticle-nanoparticle junction. However, because this represents an emerging field, the data that are available and that qualify for this review are not substantial enough to make statistically relevant conclusions about the magnitude effect of different parameters on heat flow across nanoparticle-nanoparticle interfaces. As a result, we recommend that additional benchmarking studies be done in order to establish a path forward for research in this area.

Acknowledgment

The authors gratefully acknowledge the efforts of undergraduate student Robert Fichera in producing the images in [Figure 1](#). RJW gratefully acknowledges support from the EPA STAR Fellowship program.

This material is based upon work supported by the National Science Foundation under Grant no. 0931507. Any opinions, findings, and conclusions or recommendations expressed in this material are those of the author(s) and do not necessarily reflect the views of the National Science Foundation. The research described in this paper has also been funded in part by the U.S. Environmental Protection Agency (EPA) under the Science to Achieve Results (STAR) Graduate Fellowship Program under Grant no. FP917371. EPA has not officially endorsed this publication and the views expressed herein may not reflect the views of the EPA.

References

- [1] R.J. Mehta, Y. Zhang, C. Karthik, B. Singh, R.W. Siegel, T. Borca-Tasciuc, G. Ramanath, *Nat. Mater.* 11 (2012) 233-240.
- [2] R.F. Service, *Science* 339 (2013) 263.
- [3] A.S. Arico, P. Bruce, B. Scrosati, J.-M. Tarascon, *Nat. Mater.* 4 (2005) 366-377.
- [4] P. Simon, Y. Gogotsi, *Nat. Mater.* 7 (2008) 845-854.
- [5] K.C. Krogman, T. Druffel, M.K. Sunkara, *Nanotechnology* 16 (2005) S338-S343.
- [6] A.C. Balazs, T. Emrick, T.P. Russell, *Science* 17 (2006) 1107-1110.
- [7] L. Wei, F. Yanhui, P. Jia, Z. Xinxin, *J. Heat Trans.-T ASME* 134 (2012) 092401.
- [8] A. Henry, G. Chen, *Phys. Rev. Lett.* 23 (2008) 235502-235505.
- [9] P.E. Hopkins, M. Baraket, E.V. Barnat, T.E. Beechem, S.P. Kearney, J.C. Duda, J. Robinson, S. Walton, *Nano Lett.* 12 (2012) 590-595.

- [10] M.F.L. De Volder, S.H. Tawfick, R.H. Baughman, A.J. Hart, *Science* 339 (2013) 535-539.
- [11] S. Shen, A. Henry, J. Tong, R. Zheng, G. Chen, *Nat. Nanotech.* 4 (2010) 251-255.
- [12] A. Henry, G. Chen, S.J. Plimpton, A. Thompson, *Phys. Rev. B* 82 (2010) 144308.
- [13] E. Pop, D. Mann, Q. Wang, K. Goodson, H. Dai, *Nano Lett.* 6 (2005) 96-100.
- [14] A.M. Marconnet, M.P. Panzer, K.E. Goodson, *Rev. Mod. Phys.* 85 (2013) 1296-1327.
- [15] A.A. Balandin, *Nat. Mater.* 10 (2011) 569-581.
- [16] N. Mingo, D.A. Stewart, D.A. Broido, D. Srivastava, *Phys. Rev. B* 77 (2008) 033418.
- [17] Y. Ma, R. Heijl, A.E.C. Palmqvist, *J. Mater. Sci.* 48 (2013) 2767-2778.
- [18] L. Shi, *Nanos. Microsc. Therm.* 16 (2012) 79-116.
- [19] J. Xu, T. Fisher, *Int. J. Heat Mass Transf.* 49 (2006) 1658-1666.
- [20] M. Williamson, A. Majumdar, *J. Heat Transf.-T ASME* (1992) 802-810.
- [21] A.J. McNamara, Y. Joshi, Z. Zhang, *Int. J. Therm. Sci.* 62 (2012) 2-11.
- [22] S.T. Huxtable, D.G. Cahill, S. Shenogin, L. Xue, R. Ozisik, P. Barone, M. Usrey, M.S. Strano, G. Siddons, M. Shim, P. Keblinski, *Nat. Mater.* 2 (2003) 731-734.
- [23] J.C. Duda, T.E. Beechem, J.L. Smoyer, P.M. Norris, P.E. Hopkins, *J. Appl. Phys.* 108 (2010) 073515.
- [24] P.E. Hopkins, J.C. Duda, P.M. Norris, *J. Heat Transf.* 133 (2011) 062401.
- [25] P.G. Collins, P. Avouris, *Sci. Am.* 283 (2000) 62-69.
- [26] E. Pop, K.E. Goodson, *J. Electron. Packag.* 128 (2006) 102-108.
- [27] V. Bahadur, J. Xu, Y. Liu, T.S. Fisher, *J. Heat Transf.-T ASME*, 127, 664-668.
- [28] R. Prasher, *Nano Lett.* 5 (2005) 2155-2159.
- [29] D. Singh, J.Y. Murthy, T.S. Fisher, *J. Heat Transf.-T ASME*, 133, 042402.
- [30] T.-Y. Choi, D. Poulidakos, J. Tharian, U. Sennhauser, *Nano Lett.* 6 (2006) 1589-1593.
- [31] G. Zhang, C. Liu, S. Fan, *ACS Nano* 6 (2012) 3057-3062.
- [32] Q.W. Li, C.H. Liu, S.S. Fan, *Nano Lett.* 9 (2009) 3805-3809.
- [33] R.J. Warzoha, R.M. Weigand, A. Rao, A.S. Fleischer, Experimental characterization of the thermal diffusivity of paraffin phase change material embedded with herringbone style graphite nanofibers, in: *Proceedings of the ASME Summer Heat Transfer Conference, Rio Grande, PR, (2012), 307-315.*
- [34] C. Yu, S. Saha, J. Zhou, L. Shi, A.M. Cassell, B.A. Cruden, Q. Ngo, J. Li, *J. Heat Transf.-T ASME* 128 (2006) 234-239.
- [35] F. Zhou, A. Persson, L. Samuelson, H. Linke, L. Shi, *Appl. Phys. Lett.* 99 (2011) 063110.
- [36] P. Kim, L. Shi, A. Majumdar, P.L. McEuen, *Phys. Rev. Lett.* 87 (2001) 215502.
- [37] Z. Xu, M.J. Buehler, *ACS Nano* 3 (2009) 2767-2775.
- [38] Z. Xu, M.J. Buehler, *Nano Lett.* 9 (2009) 2065-2072.
- [39] M.D. Losego, M.E. Grady, N.R. Sottos, D.G. Cahill, P.V. Braun, *Nat. Mater.* 11 (2012) 502-506.
- [40] M.I. Dafiñone, G. Feng, T. Brugarolas, K.E. Tettey, D. Lee, *ACS Nano* 5 (2011) 5078-5087.
- [41] A.B. Dalton, A. Ortiz-Acevedo, V. Zorbas, E. Brunner, W. M. Sampson, S. Collins, J.M. Razal, M.M. Yoshida, R. H. Baughman, R.K. Draper, I.H. Musselman, M. Jose-Yacamán, G.R. Dieckmann, *Adv. Funct. Mater.* 14 (2004) 1147-1151.
- [42] Y.C. Zhang, A.A. Broekhuls, M.C.A. Stuart, T.F. Landaluze, D. Fausti, P. Rudolf, F. Picchioni, *Macromolecules* 41 (2008) 6141-6146.
- [43] I. Lahiri, D. Lahiri, S. Jin, A. Agarwal, W. Choi, *ACS Nano* 5 (2011) 780-787.
- [44] M.J. Biercuk, M.C. Llaguno, M. Radosavljeć, J.K. Hyun, A.T. Johnson, *Appl. Phys. Lett.* 80 (2002) 2767-2769.
- [45] R.J. Warzoha, D. Zhang, G. Feng, A.S. Fleischer, *Carbon* 61 (2013) 441-457.
- [46] O. Sanusi, R.J. Warzoha, A.S. Fleischer, *Int. J. Heat Mass Transf.* 54 (2011) 4429-4436.
- [47] K. Chintakrinda, R.J. Warzoha, R.D. Weinstein, A.S. Fleischer, *J. Heat Transf.-T ASME* 134 (2011) 071901.
- [48] H. Babaei, P. Keblinski, J.M. Khodadadi, *Phys. Lett. A* 377 (2013) 1358-1361.
- [49] L. Fan, J.M. Khodadadi, *Renew. Sustain. Energy Rev.* 15 (2011) 24-46.
- [50] F. Yavari, H.R. Fard, K. Pashavi, M.A. Rafiee, Z. Zamiri, Z. Yu, R. Ozisik, T. Borca-Tasciuc, N. Koratkar, *J. Phys. Chem. C* 115 (2011) 8753-8758.
- [51] J.A. Eastman, S.U.S. Choi, S. Li, W. Yu, L.J. Thompson, *Appl. Phys. Lett.* 78 (2001) 718-720.
- [52] S.K. Das, S.U.S. Choi, H.E. Patel, *Heat Transf. Eng.* 27 (2006) 3-19.
- [53] N. Yang, G. Zhang, B. Li, *Nano Today* 5 (2010) 85-90.
- [54] D.P.H. Hasselman, L.F. Johnson, *J. Compos. Mater.* 21 (1987) 508-515.
- [55] R. Prasher, P. Bhattacharya, P.E. Phelan, *J. Heat Transf.-T ASME* 128 (2006) 588-595.
- [56] J. Nanda, C. Maranville, S.C. Bollin, D. Sawall, H. Ohtani, J.T. Remillard, J.M. Ginder, *J. Phys. Chem. C* 112 (2008) 654-658.
- [57] J.J. Wang, R.T. Zheng, J.W. Gao, G. Chen, *Nano Today* 7 (2012) 124-136.
- [58] J. Fan, L. Wang, *J. Heat Transf.-T ASME*, 133, 040801.
- [59] C.-W. Nan, R. Birringer, D.R. Clarke, H. Gleiter, *J. Appl. Phys.* 81 (1997) 6692-6699.
- [60] H. Babaei, P. Keblinski, J.M. Khodadadi, *J. Appl. Phys.* 113 (2013) 084302.
- [61] J.W. Gao, R.T. Zheng, H. Ohtani, D.S. Zhu, G. Chen, *Nano Lett.* 9 (2009) 4128-4132.
- [62] W. Evans, R. Prasher, J. Fish, P. Meakin, P. Phelan, P. Keblinski, *Int. J. Heat Mass Transf.* 51 (2008) 1431-1438.
- [63] A. Amrollahi, A.A. Hamidi, A.M. Rashidi, *Nanotechnology* 19 (2008) 315701.
- [64] Z. Haddad, E. Abu-Nada, H.F. Oztog, A. Mataoui, *Int. J. Therm. Sci.* 57 (2012) 152-162.
- [65] J. Buongiorno, D.C. Venerus, N. Prabhat, T. McKrell, J. Townsend, et al., *J. Appl. Phys.* 106 (2009) 094312-094326.
- [66] A. Minnich, G. Chen, *Appl. Phys. Lett.* 91 (2007) 073105.
- [67] S. Kaustav, B. Kavlicoglu, Y. Liu, F. Gordaninejad, O. A. Graeve, *J. Appl. Phys.* 106 (2009) 064307.
- [68] Z.-T. Yu, X. Fang, L.-W. Fan, X. Wang, Y.-Q. Xiao, Y. Zeng, X. Xu, Y.-C. Hu, K.-F. Cen, *Carbon* 53 (2013) 277-285.
- [69] R.J. Warzoha, A.S. Fleischer, *Int. J. Heat Mass Transf.* 71 (2014) 779-789.
- [70] R.J. Warzoha, A.S. Fleischer, *Int. J. Heat Mass Transf.* 71 (2014) 790-807.
- [71] D.-W. Oh, A. Jain, J.K. Eaton, K.E. Goodson, J.S. Lee, *Int. J. Heat Fluid Flow* 29 (2008) 1456-1461.
- [72] S. Harikrishnan, A.A. Roseline, S. Kalaiselvam, *IEE Trans. Nanotechnol.* 12 (2013) 629-635.
- [73] X. Zhang, H. Gu, M. Fujii, *J. Appl. Phys.* 100 (2006) 044325.
- [74] H. Xie, J. Wang, T. Xi, F. Ai, Q. Wu, *J. Appl. Phys.* 91 (2002) 4568-4572.
- [75] D.G. Cahill, K.E. Goodson, A. Majumdar, *J. Heat Transf.-T ASME* 124 (2002) 223-241.
- [76] S.D. Kang, S.C. Lim, E.-S. Lee, Y.W. Cho, Y.-H. Kim, H.-K. Lyeo, Y.H. Lee, *ACS Nano* 6 (2012) 3853-3860.
- [77] O.M. Wilson, X. Hu, D.G. Cahill, P.V. Braun, *Phys. Rev. B* 66 (2002) 224301.
- [78] A.P. Wemhoff, *Int. J. Heat Mass Transf.* 62 (2013) 255-262.
- [79] C.H. Li, G.P. Peterson, *J. Appl. Phys.* 99 (2006) 084314.
- [80] J.-Y. Jung, J.Y. Yoo, *Int. J. Heat Mass Transf.* 52 (2009) 525-528.

- [81] B. Barbes, R. Paramo, E. Blanco, M.J. Pastoriza-Gallego, M.M. Pineiro, J.L. Legido, C. Casanova, J. Therm. Anal. Calorim. 111 (2013) 1615-1625.
- [82] A. Amrollahi, A.A. Hamidi, A.M. Rashidi, Nanotechnology 19 (2008) 315701.
- [83] S. Harish, K. Ishikawa, E. Einarsson, S. Aikawa, S. Chiashi, J. Shiomi, S. Marayuma, Int. J. Heat Mass Transf. 55 (2012) 3885-3890.
- [84] M. Kole, T.K. Dey, J. Phys. D: Appl. Phys 43 (2010) 315501.
- [85] M. Yeganeh, N. Shahtahmasebi, A. Kompany, E.K. Goharshadi, A. Youssefi, L. Siller, Int. J. Heat Mass Transf. 53 (2010) 3186-3192.
- [86] M.B. Bryning, D.E. Milkie, M.F. Islam, J.M. Kikkawa, A.G. Yodh, Appl. Phys. Lett. 87 (2005) 161909.
- [87] R. Kothari, C.T. Sun, R. Dinwiddie, H. Wang, Int. J. Heat Mass Transf. 66 (2013) 823-829.
- [88] M.-T. Hung, O. Choi, Y.S. Ju, H.T. Hahn, Appl. Phys. Lett. 89 (2006) 023117.
- [89] I. Firkowska, A. Boden, A.-M. Vogt, S. Reich, J. Mater. Chem. 21 (2011) 17541-17546.
- [90] S. Shenogin, X. Liping, R. Ozisik, P. Keblinski, D.G. Cahill, J. Appl. Phys. 95 (2004) 8136-8144.
- [91] S.T. Huxtable, D.G. Cahill, S. Shenogin, L. Xue, R. Ozisik, P. Barone, M. Usrey, M.S. Strano, G. Siddons, M. Shim, P. Keblinski, Nat. Mater. 2 (2003) 731-734.
- [92] S. Hida, T. Hori, T. Shiga, J. Elliott, J. Shiomi, Int. J. Heat Mass Transf. 67 (2013) 1024-1029.
- [93] C.F. Carlborg, J. Shiomi, S. Maruyama, Phys. Rev. B 78 (2008) 205406.
- [94] D. Torii, T. Ohara, K. Ishida, J. Heat Transf.-T ASME (2010)1-9.
- [95] L. Xue, P. Keblinski, S.R. Phillpot, S.U.S. Choi, J.A. Eastman, Int. J. Heat Mass Transf. 47 (2004) 4277-4284.
- [96] L. Xue, P. Keblinski, S.R. Phillpot, S.U.S. Choi, J.A. Eastman, J. Chem. Phys. 118 (2003) 337-339.
- [97] R. Prasher, Appl. Phys. Lett. 94 (2009) 041905.
- [98] S. Shenogin, A. Bodapati, L. Xue, R. Ozisik, P. Keblinski, Appl. Phys. Lett. 85 (2004) 2229-2231.
- [99] J.V. Goicochea, M. Hu, B. Michel, D. Poulikakos, J. Heat Transf.-T ASME 133 (2011) 082401.
- [100] L. Chen, H. Xie, Colloids Surf. A 352 (2009) 136-140.
- [101] B.T. Branson, P.S. Beauchamp, J.C. Beam, C.M. Lukehart, J.L. Davidson, ACS Nano 7 (2013) 3183-3189.
- [102] S.S.J. Aravind, P. Baskar, T.T. Baby, R.K. Sabareesh, S. Das, S. Ramaprabhu, J. Phys. Chem. C 115 (2011) 16737-16744.
- [103] R. Gulotty, M. Castellino, P. Jagdale, A. Tagliaferro, A.A. Balandin, ACS Nano 7 (2013) 5114-5121.
- [104] S. Lin, M.J. Buehler, Nanotechnology 24 (2013) 165702.
- [105] T.C. Clancy, T.S. Gates, Polymer 47 (2006) 5990-5996.
- [106] C.-C. Teng, C.-C.M. Ma, C.-H. Lu, S.-Y. Yang, S.-H. Lee, M.-C. Hsiao, M.-Y. Yen, K.-C. Chiou, T.-M. Lee, Thermal conductivity and structure of non-covalent functionalized graphene/epoxy composites, Carbon 49 (2011) 5107-5116.
- [107] Q. Cao, H.-s. Kim, N. Pimparkar, J.P. Kulkarni, C. Wang, M. Shim, K. Roy, M.A. Alam, J.A. Rogers, Nature 454 (2008) 495-500.
- [108] S. Kim, S. Kim, J. Park, S. Ju, S. Mohammadi, ACS Nano 4 (2010) 2994-2998.
- [109] H. Zhong, J.R. Lukes, Phys. Rev. B 74 (2006) 125403.
- [110] J. Liu, M. Alhashme, R. Yang, Carbon 50 (2012) 1063-1070.
- [111] G. Domingues, S. Volz, K. Joulain, J.-J. Greffet, Phys. Rev. Lett. 94 (2005) 085901.
- [112] M. Foygel, R.D. Morris, D. Anez, S. French, V.L. Sobolev, Phys. Rev. B 71 (2005) 104201.
- [113] S. Kumar, M.A. Alam, J.Y. Murthy, Appl. Phys. Lett. 90 (2007) 104105.
- [114] J. Ordóñez-Miranda, R. Yang, J.J. Alvarado-Gil, Appl. Phys. Lett. 98 (2011) 233111.
- [115] J. Yang, S. Waltermire, Y. Chen, A.A. Zinn, T.T. Xu, D. Li, Appl. Phys. Lett. 96 (2010) 023109.
- [116] A.M. Marconnet, N. Yamamoto, M.A. Panzer, B.L. Wardle, K.E. Goodson, ACS Nano 5 (2011) 4818-4825.
- [117] P. Bonnet, D. Sireude, B. Garnier, O. Chauvet, Appl. Phys. Lett. 91 (2007) 201910.
- [118] R. Haggenueller, C. Guthy, J.R. Lukes, J.E. Fischer, K.I. Winey, Macromolecules 40 (2007) 2417-2421.
- [119] S.Y. Kwon, I.M. Kwon, Y.-G. Kim, S. Lee, Y.-S. Seo, Carbon 55 (2013) 285-290.
- [120] R.T. Zheng, J.W. Gao, J.J. Wang, G. Chen, Nat. Commun. 2 (2011).
- [121] H. Fukushima, L.T. Drzal, B.P. Rook, M.J. Rich, J. Therm. Anal. Calorim. 85 (2006) 235-238.
- [122] B.A. Cola, J. Xu, T.S. Fisher, Int. J. Heat Mass Transf. 52 (2009) 3490-3503.
- [123] Y. Won, Y. Gao, M.A. Panzer, K.E. Goodson, Proc. Natl. Acad. Sci. USA 110 (2013) 20426-20430.
- [124] Y. Gao, T. Kodama, Y. Won, S. Dogbe, L. Pan, K.E. Goodson, Carbon 50 (2012) 3789-3798.
- [125] M.T. Pettes, L. Shi, Adv. Funct. Mater. 19 (2009) 3918-3925.
- [126] M.H. Khadem, A.P. Wemhoff, J. Chem. Phys. 138 (2013) 084708.
- [127] S. Ganguli, A.K. Roy, D.P. Anderson, Carbon 46 (2008) 806-817.
- [128] X. Huang, C. Zhi, P. Jiang, D. Golberg, Y. Bando, T. Tanaka, Adv. Funct. Mater. 23 (2013) 1824-1831.
- [129] Z. Lin, A. Mcnamara, Y. Liu, K.-s. Moon, C.-P. Wong, Compos. Sci. Technol. 90 (2014) 123-128.



Ronald J. Warzoha is currently a Ph.D. student in the Mechanical Engineering Department at Villanova University. He is also a recipient of the prestigious EPA STAR Fellowship. His research interests include nanoscale energy transport, heat flow across nano-sized interfaces, waste heat energy recovery, two-phase heat and mass transfer, electronics cooling and heat conduction mechanisms in nanocomposites.



Dr. Amy S. Fleischer is a Professor of Mechanical Engineering at Villanova University where she is also Associate Chair of Mechanical Engineering and Director of Graduate Studies. She also heads the NovaTherm Research Laboratory. Her research interests include the broad topics of sustainable energy system design and thermal management of electronic systems. She has published extensively on the topics of nano-enhanced materials, energy storage in phase change materials, and waste heat recovery from data centers. Dr. Fleischer is a fellow of ASME and has chaired the ASME Technical Committee on Electronics Thermal Management (2009-2011). She was named the "2010 ASME EPPD Women Engineer of the Year Award" which recognizes a women engineer with significant technical achievements in the area of electronic and photonic packaging and was also the recipient of the 2011 ASME K-16 Clock Award for "Outstanding and continuing contributions to the science and engineering of heat transfer in electronics."